

## REVIEW

View Article Online  
View Journal | View IssueCite this: *Mater. Chem. Front.*,  
2021, 5, 4833

# Metal halide perovskite-based flexible tandem solar cells: next-generation flexible photovoltaic technology

Yan Jiang \*<sup>a</sup> and Yabing Qi \*<sup>b</sup>

Flexible solar cells, which are compatible with low cost and high throughput roll-to-roll manufacturing, are specifically attractive for applications in wearable/portable electronic devices, building-integrated photovoltaics (BIPV), drones and satellites, etc. Integration of the narrow bandgap flexible solar cells, e.g., Cu(In, Ga)(S, Se)<sub>2</sub> solar cells, organic solar cells, or the new class of lead-tin mixed perovskite solar cells (PSCs) with wide bandgap NIR-transparent PSCs allows two sub-cells to utilize solar light with different photon energies more efficiently and therefore minimizes thermalization loss to overcome the theoretical Shockley–Queisser single-junction limit (33%). In this review, we provide an overview of the recent progress of flexible perovskite-based tandem solar cells from the perspective of the narrow bandgap bottom cell and the near-infrared (NIR) transparent top cell. In addition, we discuss the key limitations related to energy losses in the recombination layer in two-terminal (2-T) tandems and the optical losses in four-terminal (4-T) tandems. Then we outline several strategies to overcome these limitations. Finally, we provide an outlook on roll-to-roll manufacturing and device encapsulation.

Received 19th February 2021,  
Accepted 20th April 2021

DOI: 10.1039/d1qm00279a

rsc.li/frontiers-materials

## 1. Introduction

According to the global agenda by the Paris COP 21 agreement, the world is transitioning to a low-carbon and sustainable society. As a promising renewable energy source, solar photovoltaic (PV) contributed to about 2% of the total global electricity in 2016 and is expected to boost to an estimated

<sup>a</sup> Energy Materials and Optoelectronics Unit, Songshan Lake Materials Laboratory, Dongguan, Guangdong 523808, China. E-mail: jiangyan@sslab.org.cn

<sup>b</sup> Energy Materials and Surface Sciences Unit (EMSSU), Okinawa Institute of Science and Technology Graduate University (OIST), Okinawa 904-0495, Japan. E-mail: Yabing.Qi@OIST.jp



Yan Jiang

next-generation high-performance energy harvesting materials and devices.

Yan Jiang is a Professor at Songshan Lake Materials Laboratory. He received his BS and PhD from Sun Yat-Sen University and Institute of Chemistry Chinese Academy of Science, respectively. Between 2015 and 2020, he worked at Okinawa Institute of Science and Technology Graduate University and Swiss Federal Laboratories for Materials Science and Technology as a postdoctoral scholar. His research focuses on



Yabing Qi

interface sciences, perovskite solar cells, lithium ion batteries, organic electronics, energy materials and devices (<https://groups.oist.jp/emssu>).

Yabing Qi is the Professor and Unit Director of the Energy Materials and Surface Sciences Unit at Okinawa Institute of Science and Technology Graduate University in Japan, and a Fellow of the Royal Society of Chemistry. He received his BS, MPhil, and PhD from Nanjing University, Hong Kong University of Science and Technology, and UC Berkeley, respectively. His research interests include surface/



weight of 25% by 2050.<sup>1</sup> The increasing demand for light-weight and flexible PV devices has become more apparent in recent years because the technology revolution and advancement of energy-consuming portable devices allow integration of the device and solar cell into a single piece. Several examples among the diverse applications of flexible solar cells are presented in Fig. 1.<sup>2–7</sup> In 2019, Samsung and Huawei produced flexible and foldable cell phones almost at the same time, making 2019 the first year of wide-spread commercial flexible electronics.<sup>8,9</sup> Flexible solar cells may hold the key to developing overall flexible self-powered portable electronics. Besides, their high-efficiency and light weight allow flexible PV devices to be used for some critical missions in space such as the utilization of solar electric propulsion for space explorations and construction of the space-based solar power (SSP), where traditional space-based PV technologies do not meet the needs from a cost perspective.<sup>10,11</sup>

Improving the power conversion efficiency (PCE) of a flexible solar cell is an ideal way to reduce the levelized cost of electricity (LCOE) of the photovoltaic (PV) system. So far, Cu(In,Ga)(S,Se)<sub>2</sub> (CIGS) and amorphous silicon (a-Si:H) are the most successful flexible solar cell technologies and are dominating the flexible PV market.<sup>12,13</sup> With several technological breakthroughs (*e.g.*, substrate optimization, optical and electronic losses reduction, bandgap grading and alkali post-deposition treatment) in the last three decades, flexible CIGS solar cells have reached a certified efficiency of 20.8% (0.51 cm<sup>2</sup> aperture area)

(Fig. 2).<sup>14–20</sup> A commercial product from MiaSolé Hi-Tech Corp shows a PCE of 17.4% on an aperture area of 0.49 m<sup>2</sup>.<sup>21</sup> The a-Si:H solar cells have a lower efficiency (16.3% in the case of the a-Si:H/a-SiGe:H/nc-Si:H triple-junction device) but the unique deposition technique, *i.e.*, plasma-enhanced chemical vapor deposition (PECVD), allows the solar cell to be directly fabricated on large-area substrates of up to 5.7 m<sup>2</sup>.<sup>13</sup> Organic solar cells (OSCs) and perovskite solar cells (PSCs) are new classes of flexible solar cell technologies holding great potential. Flexible OSCs have demonstrated a rapid technological advancement in the last two decades and reached a PCE of 14.06% (Fig. 2).<sup>22–25</sup> PSCs, a so-called game-changer in the PV field, have shown outstanding progress since the first study published in 2009 (Fig. 2).<sup>26,27</sup> Development of low-temperature processed charge transporting layers (CTLs),<sup>28,29</sup> utilizing advanced flexible electrode<sup>30</sup> and tuning perovskite composition<sup>31</sup> have led to flexible PSCs with a stabilized PCE of 19.01% on the area of lab-scale (0.1 cm<sup>2</sup>).

State-of-the-art CIGS and OSCs are narrow bandgap solar cells with absorption edges close to 1100 nm and 950 nm, respectively. High-efficiency PSCs show a tunable bandgap with an absorption edge of around 1000 nm in the case of a lead-tin mixed perovskite<sup>41</sup> and 700 nm in the case of a mixed cation (*e.g.*, FA<sup>+</sup>, MA<sup>+</sup>, Cs<sup>+</sup>) and mixed halide (*e.g.*, I<sup>-</sup>, Br<sup>-</sup>) perovskite.<sup>42</sup> Integration of the narrow bandgap flexible CIGS, OSCs, or lead-tin mixed PSCs with wide bandgap near-infrared (NIR)-transparent PSCs allows two sub-cells to utilize solar light with different photon energies more efficiently and therefore

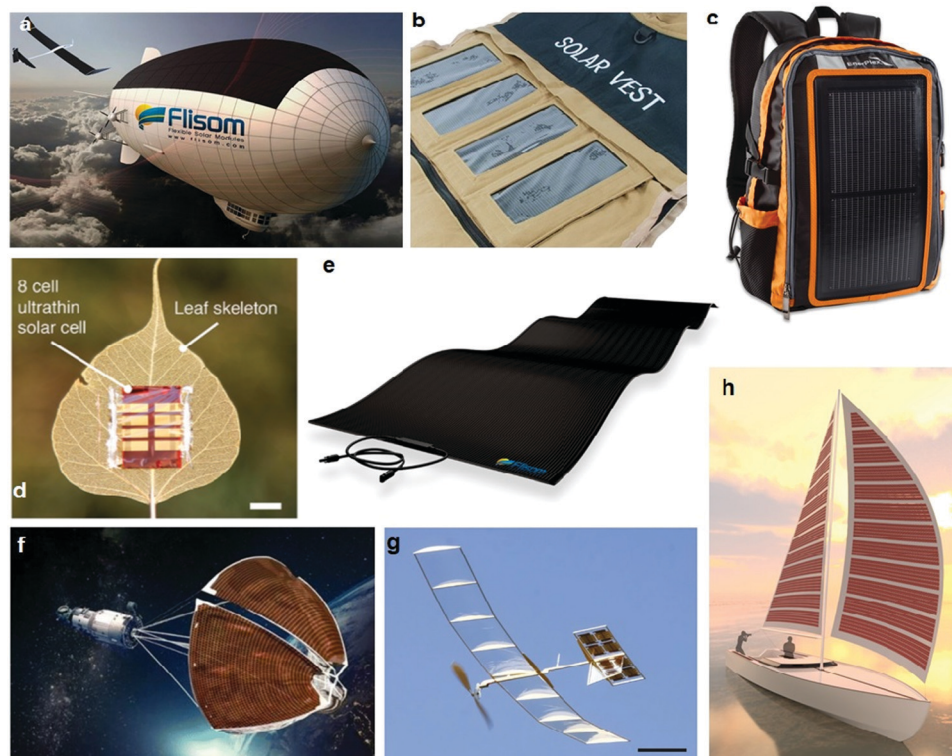


**Fig. 1** Flexible solar cells and their diverse applications. (a) Solar-powered high altitude airship,<sup>2</sup> (b) solar vest,<sup>3</sup> (c) solar recharge backpack,<sup>4</sup> (d) solar leaf,<sup>7</sup> (e) flexible solar panel,<sup>2</sup> (f) flexible perovskite solar cells for space application,<sup>5</sup> (g) solar-powered model plane,<sup>7</sup> and (h) powering a boat with printed solar.<sup>6</sup>



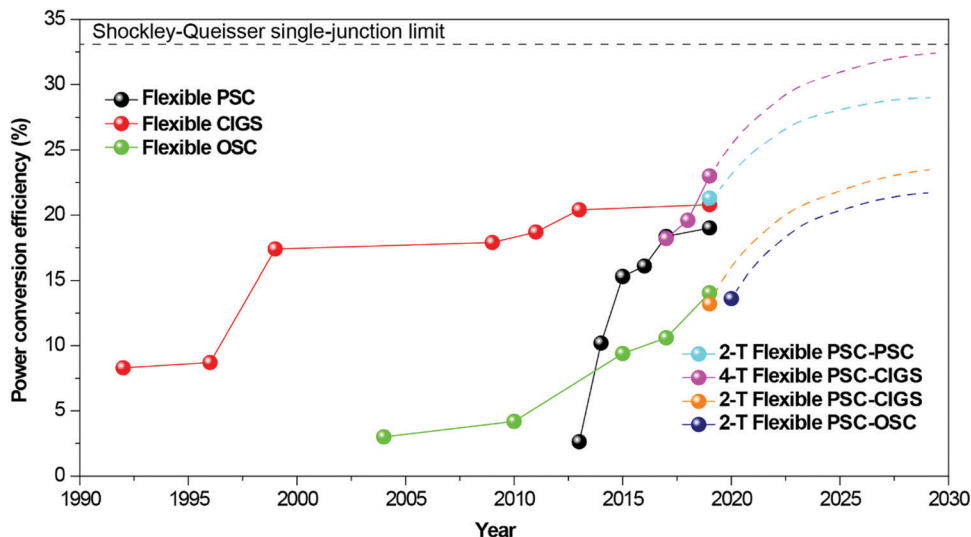


**Fig. 2** Efficiency of flexible single-junction solar cells and perovskite-based flexible tandems in 4-T and 2-T configurations. The data points are adapted from published papers on flexible perovskite solar cells,<sup>28,29,31–34</sup> flexible CIGS solar cells,<sup>14–20</sup> flexible organic solar cells,<sup>22–25</sup> 2-T flexible perovskite-perovskite tandems,<sup>35</sup> 4-T perovskite-CIGS flexible tandems,<sup>36–38</sup> 2-T flexible perovskite-CIGS tandems<sup>39</sup> and 2-T flexible perovskite-OSC tandems.<sup>40</sup> The dash lines indicate the projected efficiency evolution of various perovskite-based tandems.

minimize thermalization losses to overcome the theoretical Shockley–Queisser single-junction limit (33%). The two sub-cells can either be fabricated independently and mechanically stacked to form a four-terminal (4-T) configuration or monolithically grown with one device on top of the other to form a two-terminal (2-T) configuration. Simulated PCEs of 4-T and 2-T tandems as a function of the bandgaps of the top and bottom cells are shown in Fig. 3. Each of these two device configurations show unique advantages, which have been reported previously.<sup>43</sup> In short, 4-T tandem solar cells present fewer processing challenges and outperform 2-T tandems in terms of PCE and annual energy yield because current matching between the two sub-cells is not required. Besides, the two sub-cells are electrically insulated, meaning that one part of the device still produces power output in case of the failure of the other sub-cell.<sup>44</sup> 2-T tandem, on the other hand, is simpler in structure and the

constituent components, known as the balance of system (BOS), leading to a lower overall cost and possibly a lower LCOE.<sup>45</sup> In both tandem architectures, the optimal bandgap of the bottom absorber is slightly below 1.0 eV, corresponding to an absorption edge wavelength above 1300 nm. From the efficiency viewpoint, a flexible CIGS solar cell is the best partner for perovskite-based tandems. On the other hand, the optimal bandgap of the top cell is over 1.7 eV in the 4-T tandem and below 1.7 eV in 2-T tandems.

Although the research and development of flexible perovskite tandem solar cells are at an early stage, encouraging results have been demonstrated in several different types of combinations. By the end of 2019, the national renewable energy laboratory (NREL) reported for the first time 2-T flexible all-perovskite tandem solar cells (Fig. 2).<sup>35</sup> Integration of a nucleation layer before the recombination layer and engineering the cation composition of the wide bandgap perovskite enable

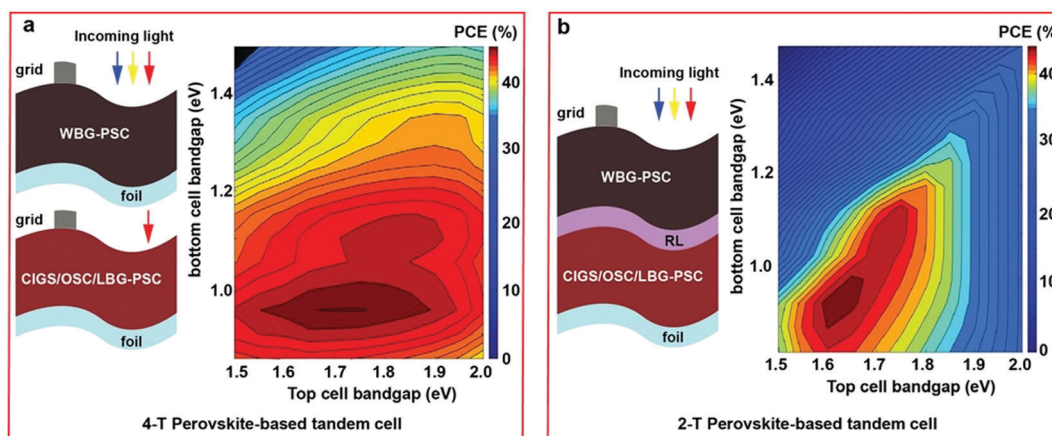


**Fig. 3** Structure and simulated efficiency of flexible tandem solar cells. (a) 4-T tandems and (b) 2-T tandems. Reproduced with permission.<sup>43</sup> Copyright 2020, Wiley-VCH.



the flexible all-perovskite tandems to achieve an efficiency of 21.3%, which is an over 2% absolute PCE improvement compared to the best single-junction flexible PSCs. In the same month, MiaSolé Hi-Tech Corp and Solliance Solar Research established a new world record PCE of 23% on a 4-T flexible perovskite-CIGS tandem solar cell, higher than the record efficiency of the sub-cells (Fig. 2).<sup>38</sup> In 2020, a 2-T perovskite-OSC tandem solar cell was reported by Wang and Zhu *et al.* by integrating a wide-bandgap perovskite (bandgap = 1.74 eV) with a narrow bandgap organic active PBDB-T:SN61C-4F (bandgap = 1.30 eV) layer. They obtained a PCE of 13.61% and a solar-to-hydrogen efficiency of 11.21% (Fig. 2).<sup>40</sup> It is rationally expected that more and more efficiency breakthroughs in perovskite tandems will be realized in the next few years.

While the PCE gain in the tandem configurations is a critical performance parameter, the additional weight and manufacturing cost of the component in a tandem solar cell should not be significant. The unique application conditions of flexible PV devices make lightweight and high flexibility prime criteria. Power-per-weight is a vital figure of merit, especially for the high-altitude and space applications when the weight of the solar cells plays a huge role. From this viewpoint, perovskite thin-film PV technologies show special advantages because the thickness of absorbers in devices is around or less than one micrometer. In 2015, Kaltenbrunner *et al.* fabricated highly flexible PSCs on transparent, commodity-scale, and ultrathin 1.4  $\mu\text{m}$ -thick PET foils (Fig. 4a).<sup>7</sup> The PSC has a total thickness of 3  $\mu\text{m}$ , including a substrate, electrodes, and a protective encapsulating layer. Using a chromium oxide-chromium interlayer and a transparent polymer electrode, the flexible PSCs realized a stabilized 12% efficiency and a record high power-per-weight of 23  $\text{W g}^{-1}$  (Fig. 4b).<sup>7</sup> This is three magnitudes higher than CIGS deposited on the glass substrate and two magnitudes higher than CIGS deposited on a polyimide (PI) substrate respectively. Flexible perovskite tandems have demonstrated an almost two-fold factor higher efficiency compared to such flexible PSC. A higher power-per-weight value could be obtained on perovskite-based tandems, especially in the case of the 2-T configuration. Energy payback time (EPBT), which is the time needed for a solar cell to generate the

Table 1 Energy payback time (EPBT) of various PV technologies

	CIGS	CdTe	OSC	PK	PK-CIGS (2T)	PK-PK (2T)
EPBT (months)	5.6	8.4–13.2	3.6–8.4	2–3	7–8(6.4)	1–1.7

The data are obtained from ref. 45,47–49.

equivalent energy consumed during manufacturing the solar cell, is another important figure of merit from the cost perspective. The EPBT is determined by several factors such as device stack, manufacturing process and solar cell efficiency, *etc.*<sup>46</sup> Solution processability and low processing temperature of state-of-the-art PSCs allow an EPBT of 2–3 months, lower than all the other flexible PV technologies such as CIGS (5.6 months), CdTe (8.4–13.2 months) or OSCs (3.6–8.4 months) (Table 1).<sup>47–49</sup> Celik *et al.* reported that 2-T PSC-CIGS tandem solar cells would realize a similar EPBT value compared to CIGS once the PCE reaches 23%.<sup>47</sup> More interestingly, they show that PSC-PSC tandems have an EPBT of only 1–1.7 months. This is the lowest value so far reported for PV devices.<sup>47</sup> Flexible perovskite-based tandems use wide-bandgap near-infrared (NIR)-transparent PSCs as the top cell and/or the narrow bandgap flexible PSC as the bottom cell. In the following two sections, we discuss the criteria and the recent progress in these two sub-cells.

## 2. Flexible NIR-transparent perovskite top cell

The function of a flexible NIR-transparent perovskite top cell is to utilize the solar energy in the UV and visible region and to allow energy in the NIR region to pass through. According to the efficiency simulation, flexible NIR transparent perovskite top cells should have a bandgap above 1.55 eV and below 1.9 eV for 4-T tandems and 1.8 eV for 2-T tandems, respectively (Fig. 3). Perovskite materials offer several advantages such as tunable bandgaps covering the target wavelength range, high absorption coefficient, sharp absorption edge and low-temperature processibility, and are ideal absorbers for flexible top cells in tandem configurations.<sup>36</sup> Efficiency, flexibility and NIR-transparency are the three key parameters for flexible

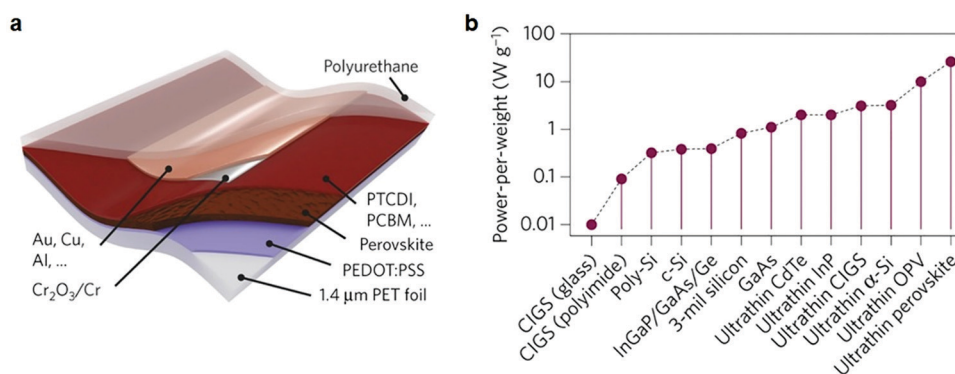


Fig. 4 Power-per-weight analysis. (a) Schematic diagram of the ultrathin perovskite solar cell. (b) Power-per-weight of various photovoltaic technologies. Reproduced with permission.<sup>7</sup> Copyright 2015, Springer Nature.



NIR-transparent PSCs. Flexible NIR-transparent PSCs have a structure of flexible substrate/bottom electrode/electron transport layer (ETL) or hole transport layer (HTL)/perovskite/HTL or ETL/top electrode. Depending on the sequence of ETL and HTL, the devices are either in an n-i-p or a p-i-n configuration. In the following sections, we overview the special manufacturing requirements for flexible PSCs compared to rigid ones and the recent progress of flexible NIR-transparent perovskite top cells.

### 2.1 Flexible substrates

The flexibility of NIR-transparent PSCs can be realized by deposition of functional layers on top of flexible and transparent substrates. So far, flexible foils such as PEN or PET are the widely used flexible substrates.<sup>50,51</sup> They are mainly polymeric materials and show several advantages including low cost, favorable bendability, high optical transparency, and chemical stability, *etc.* However, these substrates have a relatively low glass-transition ( $T_g$ ) temperature ( $<150\text{ }^\circ\text{C}$ ) and tend to deform once the temperature reaches their  $T_g$ .<sup>52</sup> To overcome this challenge, a series of low-temperature manufacturing processes have been developed for the deposition of every single layer in PSCs. As a result, whole low-temperature processed PSCs have been reported with a promising PCE.<sup>30</sup> On the other hand, flexible foils show a high water vapor transmission rate (WVTR) and oxygen transmission rate (OTR).<sup>53–56</sup>  $\text{H}_2\text{O}$  and  $\text{O}_2$  are well-known environmental impacts causing degradation of perovskite materials.<sup>11,57–59</sup> Long-term operational stability of flexible NIR-transparent PSCs using flexible foils is a potential issue. Encapsulation of flexible NIR-transparent PSCs becomes a necessity. Ultra-thin glass is another flexible substrate candidate showing higher transparency, lower  $\text{H}_2\text{O}$  and  $\text{O}_2$  permeability than the flexible foils, and can withstand an annealing temperature up to  $600\text{ }^\circ\text{C}$ .<sup>60</sup> However, the relatively high price and brittle behavior may become an issue for industrial production on a large scale.

### 2.2 Flexible and transparent electrodes

Optical transparency, electrical conductivity and mechanical robustness against bending, deformation, twisting and stretching are basic requirements for flexible and transparent electrodes. Transparent conductive oxides (TCOs) are the most successful electrode materials that can be deposited by industrial relevant magnetron sputtering methods.<sup>43</sup> However, several issues exist in state-of-the-art TCOs in view of flexible tandem applications, limiting the device performance and robustness. First, to obtain the best optical and electrical performance, a post-deposition-annealing treatment is usually required for TCOs. The high annealing temperature is usually not compatible with the flexible substrates.<sup>36</sup> Second, most of the TCOs developed for single-junction solar cells (*e.g.*, ITO and FTO) are highly degenerated n-type semiconductors with a carrier density on the order of  $10^{21}\text{ cm}^{-3}$ .<sup>61</sup> Because of free-carrier intra-band absorption, significant parasitic absorptions appear in the NIR wavelength range (800–1300 nm), accounting for a total photocurrent loss of several  $\text{mA cm}^{-2}$  in perovskite tandems.<sup>43</sup> Third, most of the high-performance TCOs, *e.g.*, indium doped tin oxide (ITO) are highly

crystalline materials, resulting in poor mechanical robustness. Cracks form in the TCO layers after bending the flexible PSCs at a small radius, which can cause a severe increase in the sheet resistance. In the last years, high-mobility and amorphous TCOs with low processing temperatures such as indium zinc oxide (IZO)<sup>37</sup> and hydrogenated indium oxide (IO:H)<sup>62</sup> have been investigated, laying the foundation for breakthroughs in flexible NIR-transparent PSCs. Besides TCOs, electrode materials that have been utilized in other types of flexible solar cells may also be suitable for flexible NIR transparent PSCs. These electrodes include conductive polymers,<sup>63</sup> thin metallic layers,<sup>64</sup> a stack of a dielectric-thin metallic layer-dielectric (DTD) structure,<sup>65</sup> transparent carbon-based electrodes (graphene<sup>30</sup> and nanotubes<sup>66</sup>) and silver nanowires, *etc.*<sup>67,68</sup>

### 2.3 Recent progress in flexible NIR transparent PSCs

In 2017, Pisoni *et al.* employed a low-temperature vacuum-based approach to grow  $\text{MAPbI}_3$  perovskite on a flexible substrate that is generally used to encapsulate flexible CIGS (Fig. 5a).<sup>35</sup> The flexible substrate shows an ultra-low water vapor transmission rate (WATR) and good UV blocking properties. They demonstrated the first flexible and NIR-transparent PSC (flexible foil/AZO/ZnO/ $\text{C}_{60}$ /MAPbI<sub>3</sub>/Spiro/MoO<sub>x</sub>/IO:H/(Ni–Al grid)) with an average transmittance of 78% between 800 and 1000 nm and a PCE of 12.2% on an area of  $0.213\text{ cm}^2$  (Fig. 5b and c). Integration with a flexible CIGS to form the 4T Pero-CIGS tandem cell resulted in a PCE of 18.2%. In 2018, Pisoni *et al.* developed a multi-stage approach to deposit perovskite absorbers that allow tailoring of the lead halide growth and perovskite crystallization kinetics.<sup>37</sup> They used sputtered IZO as the top and bottom electrodes and prepared a flexible PSC with a structure of flexible foil/IZO/PEIE/ $\text{C}_{60}$ /MAPbI<sub>3</sub>/Spiro-MeOTAD/MoO<sub>x</sub>/IZO/(Ni–Al grid) (Fig. 5d). The amorphous nature of IZO enables PSCs to obtain high mechanical robustness against bending at small radii of 6 and 4 mm. They further demonstrated a 4T PSC-CIGS flexible tandem solar cell with a PCE of 19.6%. In 2019, Hu *et al.* developed a conductive and robust network PEDOT:PSS electrode by combining an ionic additive-conductivity and flexibility enhancer (PEDOT:PSS:CFE) (Fig. 5g).<sup>63</sup> The electrode displays high conductivity over  $4100\text{ S cm}^{-1}$  and high transmittance over 85% (Fig. 5h). Using the conductive polymer as the top and bottom transparent electrodes and a mixed halide perovskite as the absorber, they fabricated a flexible semi-transparent PSC with a PCE of 12.5%, excellent mechanical flexibility, and long-term stability (Fig. 5i). In 2019, a record PCE of 21.5% on an area of  $0.09\text{ cm}^2$  was released by Solliance and MiaSolé.<sup>69</sup> In 2020, Solliance and MiaSolé announced a flexible 4T tandem device with a new record PCE of 23%.<sup>38</sup> So far, no details on these devices have been revealed. Li *et al.* showed that energy level alignment between a perovskite and charge transport layers plays a significant role in determining nonradiative recombination loss. By constructing gradient energy level alignments at both electron- and hole-selective contacts, they obtained a flexible semitransparent 1.75 eV wide-bandgap PSC with an efficiency of 15.02% and NIR transparency of around 70% (Table 2).<sup>70</sup>



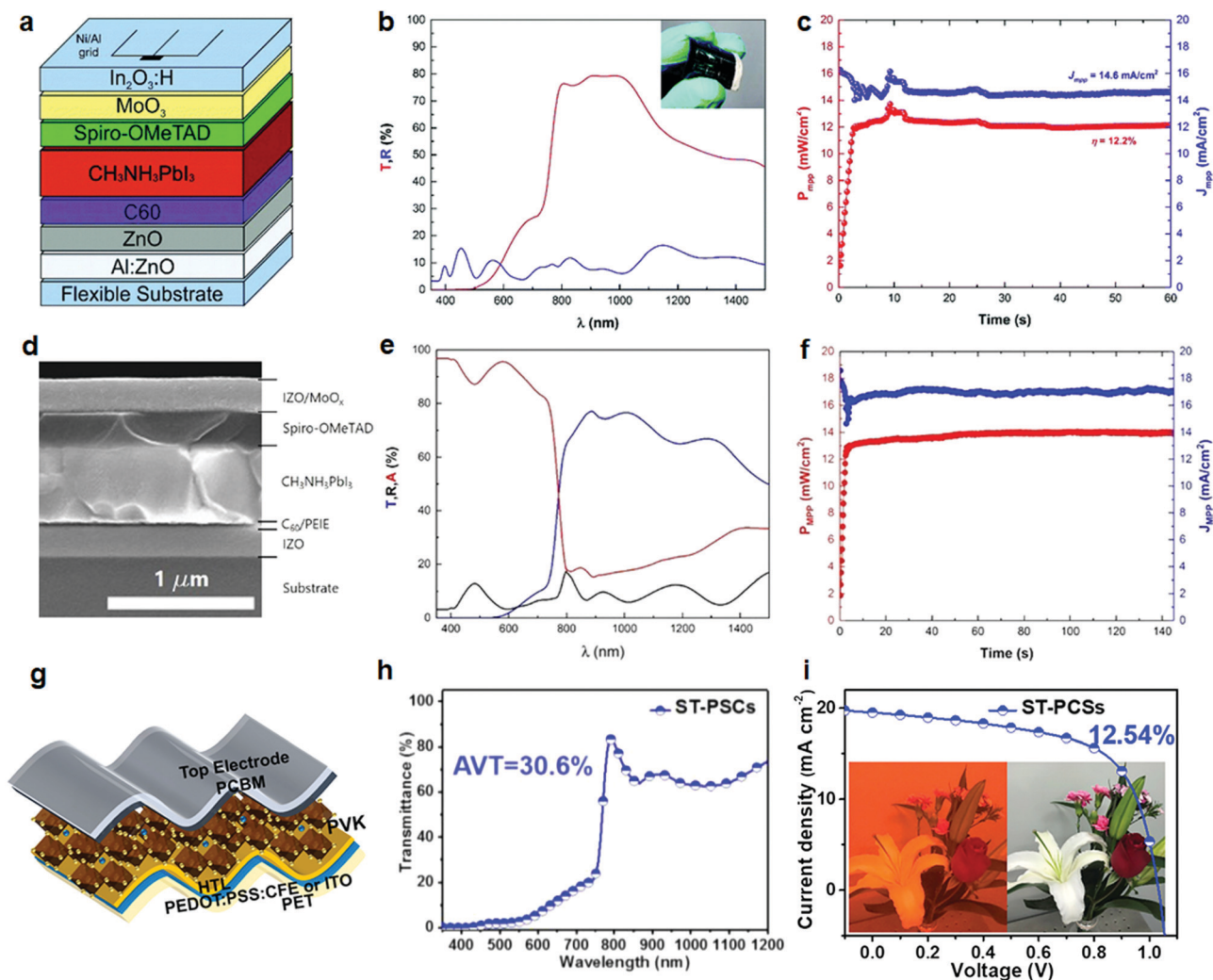


**Fig. 5** Flexible NIR-transparent perovskite solar cell. (a) Schematic diagram, (b) transmittance and reflectance curves through the entire device stack, and (c) steady-state efficiency of the flexible NIR transparent PSC. (d) Cross-section SEM image, (e) transmittance, reflectance and absorbance curves, and (f) steady-state efficiency of the flexible NIR transparent PSC. (g) Configuration of the flexible NIR transparent PSC, and (i) current–voltage curve of the flexible NIR transparent PSC. The insets in (i) show photographs taken through the NIR-transparent perovskite solar cell. (a–c) Reproduced with permission.<sup>36</sup> Copyright 2017, the Royal Society of Chemistry. (d–f) Reproduced with permission.<sup>37</sup> Copyright 2018, Springer Nature. (g–i) Reproduced with permission.<sup>63</sup> Copyright 2019, Elsevier Inc.

In 2019, Palmstrom *et al.* reported an exciting result on flexible and all-perovskite monolithic tandems.<sup>35</sup> They partially substituted Cs with dimethylammonium (DMA) in mixed halide perovskite, leading to a 1.7 eV bandgap perovskite with a high and stable  $V_{oc}$  of 1.2 V (Fig. 6a–c). Furthermore, they

implemented a 1 nm-thick poly(ethylenimine)ethoxylated (PEIE) nucleation layer that enables a conformal coating of crystallized aluminum zinc oxide recombination layer (Fig. 6d). Such a recombination layer efficiently combines the two sub-cells and prevents damage to the bottom cell when processing the top

**Table 2** Summary of flexible NIR transparent PSCs

Device structure	$V_{oc}$ (V)	$J_{sc}$ (mA cm <sup>-2</sup> )	FF (%)	$\eta$ (%)	$\eta_{mpp}$ (%)	Area (cm <sup>2</sup> )	NIR T (%)	Year	Ref.
Foil/AZO/ZnO/C <sub>60</sub> /MAPbI <sub>3</sub> /Spiro-MeOTAD/MoO <sub>x</sub> /IO:H/(Ni–Al grid)	1.08	16.1	68.5	11.9	12.2	0.285	78	2017	36
Sub/IZO/PEIE/C <sub>60</sub> /MAPbI <sub>3</sub> /Spiro-MeOTAD/MoO <sub>x</sub> /IZO/(Ni–Al grid)	1.06	18.7	68.9	13.7	14	0.27	74	2018	37
PET/n-PEDOT:PSS/FA <sub>1-x</sub> MA <sub>x</sub> PbI <sub>3</sub> /Spiro-MeOTAD/n-PEDOT:PSS	0.99	17.3	60	10.3	NA	0.11	60–80	2018	71
(PET)/TETA-doped GR (TETA-GR)/ZnO/MAPbI <sub>3</sub> /poly-triarylamine and the PEDOT:PSS/TFSA-doped GR (TFSA-GR)/PET stacks	0.94	18.4	64.87	11.22	NA	1	<70	2018	72
PET/PEDOT:PSS:CFE/PEDOT:PSS/PVK/PCBM/PEDOT:PSS:CFE	NA	NA	NA	NA	12.5	0.1	NA	2019	63
PET/ITO/CyDTA/SnO <sub>2</sub> /C–SnO <sub>2</sub> /perovskite/spiro-OMeTAD/MoO <sub>x</sub> /ITO.	1.186	16.35	77.5	15.02	13	0.07	70	2020	70



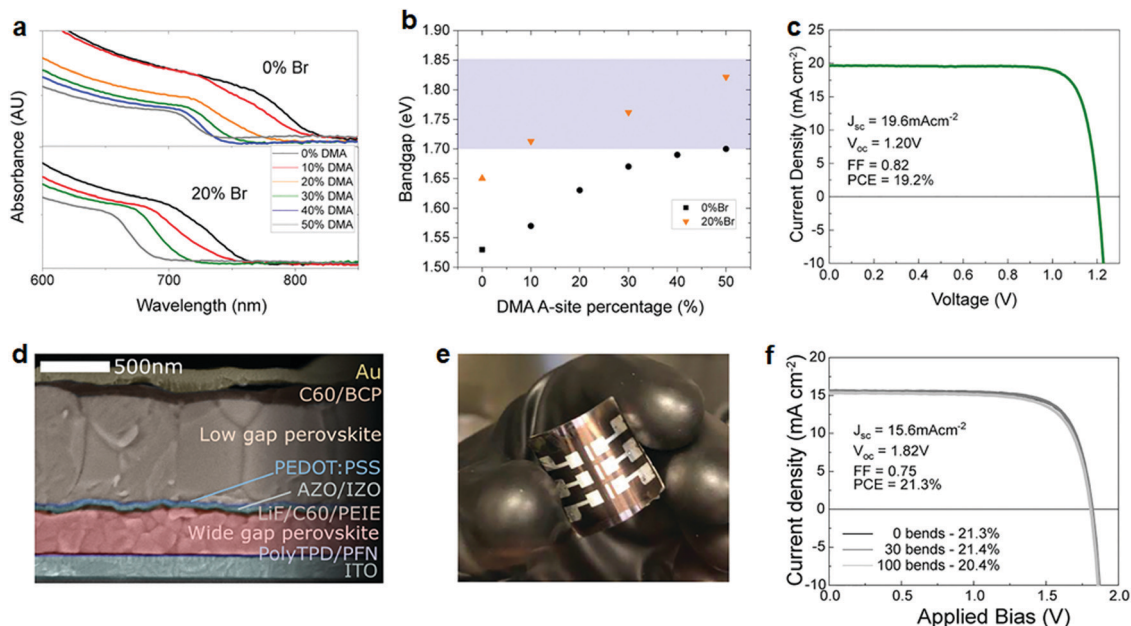


Fig. 6 Stable wide bandgap PSC for flexible tandems. (a) Absorbance spectra and (b) bandgap of perovskite with different DMA ratios in the A-site. Compositions of the perovskite layers are  $\text{FA}_{0.725(1-x)}\text{Cs}_{0.275(1-x)+0.5x}\text{DMA}_{0.5x}\text{PbI}_3$  and  $\text{FA}_{0.725(1-x)}\text{Cs}_{0.275(1-x)+0.5x}\text{DMA}_{0.5x}\text{PbI}_{2.4}\text{Br}_{0.6}$ . DMA refers to dimethylammonium iodide. (c) Current–voltage characteristics of the champion PSC (10% DMA, 20% Br). (d) Cross-section SEM image, (e) photograph and (f) current–voltage characteristics of the flexible all-perovskite tandem solar cell. (a–f) Reproduced with permission.<sup>55</sup> Copyright 2019, Elsevier Inc.

cell. The flexible and all-perovskite monolithic tandems deposited on a PEN substrate achieved a PCE of 21.4% (Fig. 6e, f). The all-perovskite flexible monolithic tandem may hold the potential for the development of high-efficiency flexible tandem solar cells with ultra-low EPBT.

### 3. Progress in narrow bandgap perovskite bottom cells

#### 3.1 Sn-based perovskite solar cell

The narrow bandgap sub-cell in a tandem solar cell absorbs lower energy photons and extends the absorption edge of a tandem device to the NIR region. A practical approach to reducing the bandgap of perovskite is to substitute Pb with Sn. Sn-based perovskites have a similar isoelectronic configuration of  $s^2p^2$  compared to the Pb-based perovskites but a smaller optical bandgap.<sup>73</sup> In 2014, Snaith *et al.* reported the first methylammonium tin iodide ( $\text{CH}_3\text{NH}_3\text{SnI}_3$ ) perovskite solar cells on glass substrates with a PCE of 6.4%. The bandgap of  $\text{CH}_3\text{NH}_3\text{SnI}_3$  is 1.23 eV, derived from the absorption spectra.<sup>74</sup> Key limits of Sn-based perovskite are the relative low formation energy of  $\text{Sn}^{2+}$  vacancy and the tendency of oxidation to  $\text{Sn}^{4+}$ , resulting in a highly conductive p-type behavior.<sup>75</sup> Additives such as 5-AVAI,<sup>76</sup>  $\text{SnF}_2$ , *etc.*,<sup>77,78</sup> are developed to mitigate the  $\text{Sn}^{2+}$  oxidation issue. Wu *et al.* introduced Lewis base molecules in the precursor solution that can efficiently tune the crystallization kinetics. They fabricated a pinhole-free  $\text{FASnI}_3$  absorber which showed a PCE of 10.1% in PSCs.<sup>79</sup> In 2019, Xi *et al.* developed a multichannel interdiffusion method to prepare uniform  $\text{FASnI}_3$  films. They for

the first time demonstrated flexible Sn-based PSCs on flexible polyethylene naphthalate (PEN) substrates with a PCE reaching 3.12% (Fig. 7a).<sup>80</sup>

#### 3.2 Mixed Sn–Pb perovskite solar cell

Mixed Sn–Pb iodide perovskite alloy, *e.g.*,  $\text{MAPb}_x\text{Sn}_{1-x}\text{I}_3$  is another promising narrow bandgap absorber candidate. Interestingly, the bandgap of the alloy is lower than  $\text{MAPbI}_3$  and  $\text{MASnI}_3$ , showing a bandgap bowing effect (Fig. 7b). This makes mixed Sn–Pb perovskite a better bottom cell for perovskite tandems in view of the theoretical PCE (Fig. 3). The reason for this abnormal behavior has been investigated by various researching groups. Several explanations such as composition-induced crystal structure variations<sup>81</sup> and short-range ordering of Pb and Sn ions<sup>41</sup> have been proposed. Goyal *et al.* applied electronic structure calculations at different levels of theory to investigate the origin of the nonlinear bandgap behavior. The results indicate that the bandgap bowing effect is because of the mismatch in energy between the s and p orbitals of Pb and Sn, which forms the band edges of the alloy (Fig. 7c).<sup>82</sup> The lowest bandgap of mixed Sn–Pb is around 1.2 eV for  $\text{MASn}_{1-x}\text{PbI}_3$  where x values equal to 0.25 and 0.5. With great research efforts devoted to the field, the PCE of the mixed Sn–Pb PSCs on glass substrates boosts from 10.1% in 2014 to 21.1% in 2020 (Fig. 7a and Table 3).<sup>83</sup> PEDOT:PSS, although found to cause device degradation, is the commonly used HTL to deliver high-efficiency narrow bandgap PSCs. In 2020, Chen *et al.* reported an exciting result by substituting PEDOT:PSS with a room temperature-processed  $\text{NiO}_x$  HTL based on nanocrystals. The  $\text{NiO}_x$  HTL shows a deeper valence band and lower trap density than high-temperature processed  $\text{NiO}_x$ , leading to



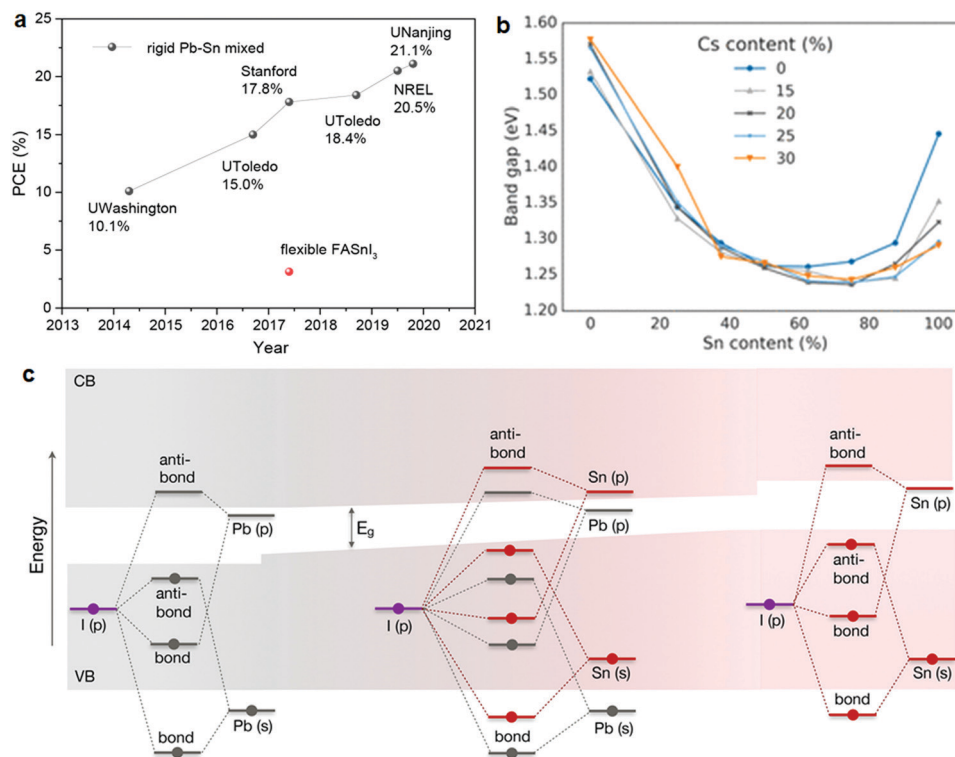


**Fig. 7** Flexible narrow bandgap PSC. (a) Efficiency evolution of the Pb–Sn mixed PSCs on rigid substrates and a flexible FASnI<sub>3</sub> PSC. (b) Bandgap variation of the mixed Sn–Pb perovskites with different Cs ratios, (c) origin of the bandgap bowing in MA(Pb<sub>1-x</sub>Sn<sub>x</sub>)I<sub>3</sub> from the molecular orbital point of view. (a) Reproduced with permission.<sup>83</sup> Copyright 2020, Wiley-VCH. (b) Reproduced with permission.<sup>90</sup> Copyright 2017, American Chemical Society. (c) Reproduced with permission.<sup>82</sup> Copyright 2018, American Chemical Society.

a PCE of 18.77% for narrow bandgap PSCs.<sup>84</sup> So far flexible mixed Sn–Pb PSCs have rarely been reported because the widely used flexible substrates for the fabrication of PSCs have high WATR and OTR. It is technically challenging to prevent the oxidation of Sn<sup>2+</sup> to Sn<sup>4+</sup>. Implementation of low WATR and OTR flexible substrates may hold the key to developing flexible mixed Sn–Pb PSCs.

#### 4. Energy losses in the recombination junction of 2-T perovskite tandems

Recombination junction, also called interconnection or tunneling junction, is a typical structure in the 2-T tandem solar cell

that physically and electrically connects the two sub-cells. Under illumination, electrons and holes are continuously generated from the two sub-cells. Photo-generated electrons transfer to the conduction band minimum and holes to the valence band maximum. Electron tunneling happens through forbidden regions into empty states, allowing the electrons and hole to recombine in the recombination junction (Fig. 8a). A typical recombination junction is a heavily doped p<sup>+</sup>-n<sup>+</sup> junction.<sup>91,92</sup> Different from a p-n junction where a high resistive and wide depletion region is created, the p<sup>+</sup>-n<sup>+</sup> junction forms a narrow depletion region with atomic width,<sup>93</sup> enabling the tunneling current to flow at a small bias voltage (Fig. 8b).

In perovskite-based tandems, the recombination junction usually consists of ETL and HTL from the perovskite sub-cell

**Table 3** Summary of narrow bandgap PSCs

Device structure	Bandgap (eV)	V <sub>oc</sub> (V)	J <sub>sc</sub> (mA cm <sup>-2</sup> )	FF (%)	η (%)	η <sub>mpp</sub> (%)	Area (cm <sup>2</sup> )	Year	Ref.
Glass/FTO/c-TiO <sub>2</sub> /meso-TiO <sub>2</sub> /CH <sub>3</sub> NH <sub>3</sub> SnI <sub>3</sub> /Spiro-MeOTAD/Au	1.23	0.88	16.8	42	6.4	—	0.12	2014	74
Glass/ITO/PEDOT:PSS/CH <sub>3</sub> NH <sub>3</sub> SnI <sub>3</sub> /PCBM/Ag	1.23	0.57	20.68	66	7.78	—	0.09	2020	78
Glass/ITO/PEDOT:PSS/FASnI <sub>3</sub> /C <sub>60</sub> /BCP/Ag	1.4	0.64	21.83	73.9	10.32	10.1	0.09	2020	79
PEN/ITO/PEDOT:PSS/FASnI <sub>3</sub> /C <sub>60</sub> /BCP/Ag	1.4	0.31	16.07	62.6	3.12	—	0.09	2017	80
glass/ITO/PEDOT:PSS/MAPb <sub>0.85</sub> Sn <sub>0.15</sub> I <sub>3-x</sub> Cl <sub>x</sub> /PCBM/C <sub>60</sub> /Ag	1.4	0.77	19.5	67.0	10.1	—	0.03	2014	85
Glass/ITO/PEDOT:PSS/(FASnI <sub>3</sub> ) <sub>0.6</sub> (MAPbI <sub>3</sub> ) <sub>0.4</sub> /C <sub>60</sub> /BCP/Ag	1.25	0.853	28.5	72.5	17.6	—	0.085 to 0.12	2017	86
Glass/ITO/PEDOT:PSS/(FASnI <sub>3</sub> ) <sub>0.6</sub> (MAPbI <sub>3</sub> ) <sub>0.4</sub> /C <sub>60</sub> /BCP/Ag	1.25	0.841	29.0	74.4	18.1	—	0.105	2018	87
Glass/ITO/PEDOT:PSS/(FASnI <sub>3</sub> ) <sub>0.6</sub> (MAPbI <sub>3</sub> ) <sub>0.4</sub> /C <sub>60</sub> /BCP/Ag	1.25	0.834	30.4	80.8	20.5	20.2	0.105	2019	88
Glass/ITO/PEDOT:PSS/FA <sub>0.7</sub> MA <sub>0.3</sub> Pb <sub>0.5</sub> Sn <sub>0.5</sub> I <sub>3</sub> /C <sub>60</sub> /BCP/Cu	1.22	0.831	31.4	80.8	21.1	20.9	0.049	2019	89
Glass/ITO/NiO <sub>x</sub> /(FASnI <sub>3</sub> ) <sub>0.6</sub> (MAPbI <sub>3</sub> ) <sub>0.4</sub> /C <sub>60</sub> /BCP/Ag	1.25	0.82	29.6	77.2	18.77	18.4	0.04	2020	84



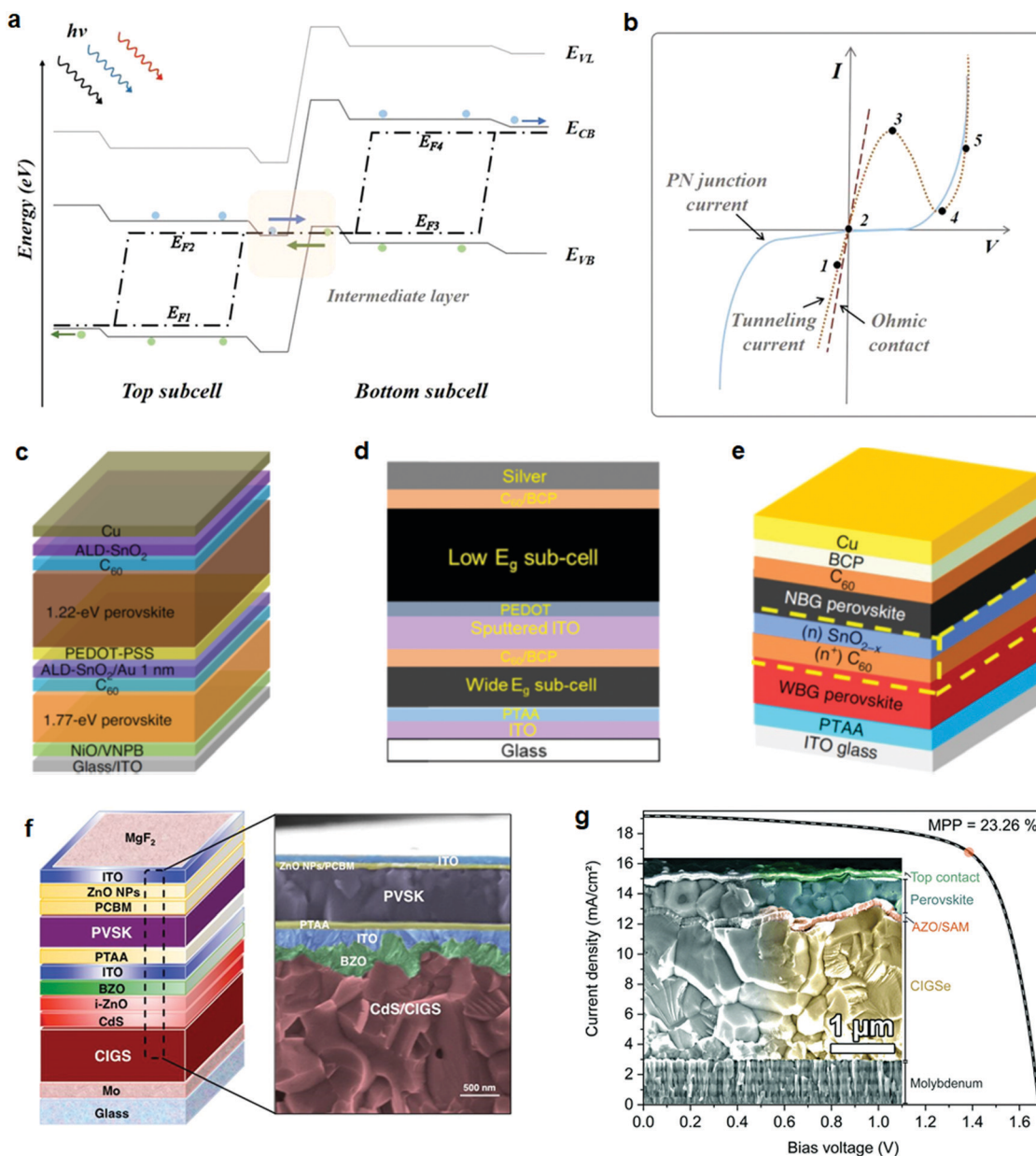


**Fig. 8** Tunneling junction in a perovskite tandem solar cell. (a) Energy level diagram of a tandem solar cell connected *via* a recombination layer and (b) current–voltage curves at the tunneling junction with respect to a p–n junction and an ohmic contact. (c–e) Schematic drawing of perovskite–perovskite tandems. The tunneling junctions are  $\text{SnO}_2/\text{Au}/\text{PEDOT:PSS}$  in (c),  $\text{ITO}/\text{PEDOT}$  in (d) and  $(n^+) \text{C}_{60}/(n) \text{SnO}_{2-x}$  in (e). (f and g) Schematic drawing and SEM images of perovskite–CIGS tandems. The tunneling junctions are  $\text{ITO}/\text{PTAA}$  in (f) and  $\text{AZO}/\text{SAM}$  in (g). (a) Reproduced with permission.<sup>100</sup> Copyright 2020, Wiley–VCH. (b) Reproduced with permission.<sup>101</sup> Copyright 1974, American Chemical Society. (c) Reproduced with permission.<sup>94</sup> Copyright 2020, Springer Nature. (d) Reproduced with permission.<sup>95</sup> Copyright 2020, Springer Nature. (e) Reproduced with permission.<sup>96</sup> Copyright 2020, Springer Nature. (f) Reproduced with permission.<sup>98</sup> Copyright 2018, the American Association for the Advancement of Science. (g) Reproduced with permission.<sup>99</sup> Copyright 2019, the Royal Society of Chemistry.

that is not a highly-degenerated semiconductor. Direct contact of the ETL with the  $p^+$  layer or the HTL with the  $n^+$  layer may result in high contact resistivity and therefore the unbalanced electron and hole populations on two sides of the recombination junction. A substantial resistive loss will be encountered, decreasing  $V_{oc}$  and FF of the tandem device. A thin layer of metal or TCO is usually implemented as part of the recombination junction to aid in carrier recombination *via* a trap-assisted

tunneling (TAT) channel.<sup>93</sup> Xiao *et al.* used a 20 nm-thick  $\text{SnO}_2$  film by atomic layer deposition (ALD) as the ETL of a PSC. They thermally evaporated a 1 nm-thick Au layer between the n-type  $\text{SnO}_2$  and the p-type PEDOT:PSS. The  $\text{SnO}_2/\text{Au}/\text{PEDOT:PSS}$  recombination junction facilitates electron–hole recombination and results in a tandem PCE of 24.8% (Fig. 8c).<sup>94</sup> Li *et al.* deposited a 130 nm-thick ITO between the ETL of  $\text{C}_{60}/\text{BCP}$  and HTL of PEDOT:PSS to construct the



recombination junction, and their all-perovskite tandems show a  $V_{oc}$  of 1.043 V, a FF of 79.3% and a PCE of 23.3% (Fig. 8d).<sup>95</sup> Yu *et al.* developed a  $C_{60}/SnO_{1.76}$  recombination junction structure. The presence of a large density of  $Sn^{2+}$  allows  $SnO_{2-x}$  to show ambipolar carrier transport property and forms ohmic contacts with adjacent layers from the two sub-cells (Fig. 8e).<sup>96</sup> Their all-perovskite tandems using the  $C_{60}/SnO_{1.76}$  recombination junction structure obtained a PCE of 24.4%.

From the energy loss perspective, some critical criteria for development of recombination layers include (i) excellent out-of-plane conductivity for efficiency electron-hole recombination; (ii) limited lateral conductivity to avoid unwanted shunting paths; (iii) have a minimum optical absorption in the NIR region. With these aims, Palmstrom *et al.*, used a highly resistive IZO to construct a recombination junction with a structure of  $C_{60}/PEIE/AZO/IZO/PEDOT:PSS$ . They reported the first flexible and all-perovskite monolithic tandems with a PCE of 21.3%.<sup>35</sup>

From the manufacturing point of view, the tunneling junction physically connects the two sub-cells. Deposition of uniform and high-electric-quality charge-transport layers and absorber in the top cell relies on the suitable recombination layer. PSC-CIGS 2-T tandem is a promising flexible solar cell technology. Generally, a high-quality CIGS absorber displays a rough surface (roughness is on the hundred-nanometer level). Because the functional layers in PSCs are a few tens to hundreds of nanometers, it is a challenge to achieve the conformal deposition of these layers on top of the rough CIGS surface. Jošt *et al.* systematically optimized the recombination junction from  $ZnO/PTAA$  to  $ZnO/NiO_x$  and  $ZnO/NiO_x/PTAA$ , and realized a conformal coating of  $NiO_x$  on top of the rough CIGS bottom cell. The efficiency of the 2-T PSC-CIGS tandems on a glass substrate improves from 3.1% to 21.6%.<sup>97</sup> Han *et al.* developed a boron-doped  $ZnO(BZO)/ITO/PTAA$  recombination junction. The ITO layer was chemical-mechanically polished to realize a smooth surface (Fig. 8f).<sup>98</sup> The advancement in recombination junction design leads to a PSC-CIGS 2-T tandem solar cell with an efficiency of 22.4%. In 2019, Al-Ashouri *et al.* used a self-assembled monolayer (SAM) of [2-(3,6-dimethoxy-9H-carbazol-9-yl)ethyl]phosphonic acid (MeO-2PACz) as an AZO surface modifier and eliminated PTAA HTL. The SAMs create an energetically aligned interface to the perovskite absorber with negligible non-radiative losses, resulting in a PSC-CIGS 2-T tandem with an efficiency of 23.3% (Fig. 8g).<sup>99</sup>

## 5. Optical losses in the flexible 4-T perovskite tandems

Flexible 4-T perovskite tandems have three transparent electrodes and several air/flexible substrate interfaces. Parasitic absorption losses in the TCOs and broadband reflection losses at the air/flexible substrate interfaces account for a total current loss of 4–5  $mA\ cm^{-2}$ .<sup>43</sup> Mitigation of these optical losses holds the key to enhancing the photocurrent and the overall performance of flexible 4-T tandems.

### 5.1 Parasitic absorption loss in transparent conductive oxides

Transparent conductive oxides are the most common electrode materials for flexible perovskite and tandem solar cells. State-of-the-art TCOs such as FTO and ITO offer superior conductivity and high transparency in the visible region (400–800 nm). However, significant parasitic absorptions appear in the NIR wavelength range (800–1300 nm), owing to free-carrier intra-band absorption (FCA). Take the commercial ITO as an example, absorbance of a 200 nm-thick ITO film reaches 18% at a wavelength of 1000 nm.<sup>62</sup> Considering that the low-energy photons should pass through three TCO layers before reaching the absorber of the narrow bandgap cell, a huge absorption loss is created and transformed to heat waste. To mitigate the FCA losses while maintaining high carrier conductivity, high carrier mobility TCOs are urgently needed. In addition, these TCOs should be deposited and post-annealed at a low temperature, *i.e.*, <150 °C to be compatible with flexible substrates.

In the last years, a series of TCO layers such as tungsten and hydrogen doped indium oxide (IWO:H), cerium and hydrogen doped indium oxide (ICO:H), zirconium-doped indium oxide (IZrO) *etc.*, have been developed, showing high electrical conductivity and small NIR absorbance of less than 2%.<sup>102</sup> In 2020, Jiang *et al.*, developed an  $In_2O_3:H$  (IO:H) film deposition process by independently controlling  $H_2$  and  $O_2$  gas flows during magnetron sputtering.<sup>62</sup> Tuning the  $H_2$  and  $O_2$  partial pressures allows decreasing the crystallization temperature to 130 °C, making it suitable for flexible substrates. Optical loss analysis suggests that replacing the state-of-the-art rear IZO of the PSC and front IZO of the  $CuInSe_2$  (CIS) with the low-temperature processed IO:H electrode leads to a 1.38  $mA\ cm^{-2}$  short-circuit current ( $J_{sc}$ ) gain in the bottom cell (Fig. 9a–c).

Besides, incorporation of metallization schemes is a powerful strategy that has been widely employed in thin-film solar cells such as CIGS and CdTe. A well-designed high-conductivity metal grid with minimal shadowing losses could be deposited on TCOs to enable reduced thickness while maintaining high conductivity.<sup>103</sup>

### 5.2 Reflection losses at the device/air interfaces

Reflective losses at the cell/air interface account for around 10% of the total available photocurrent from the AM 1.5 solar spectrum.<sup>103</sup> Previous reports on reflective loss are mostly obtained on non-flexible solar cells, where the interface is an air/glass substrate. Stefano *et al.* investigated the reflective loss at the air/flexible PSC interfaces. The device has a structure of flexible foil/ $IZO/C_{60}/PEIE/MAPbI_3/Spiro-MeOTAD/MoO_x/IZO/(Ni-Al\ grid)$  (Fig. 9d).<sup>37</sup> Experimental and simulation results reveal a significant reflection loss between 450 nm and 500 nm (Fig. 9e). A total reflection loss between 380–800 nm accounts for 1.8  $mA\ cm^{-2}$ . Several strategies have been attempted to mitigate reflection losses. (I) Deposition of an anti-reflective coating (ARC) with a refractive index intermediate between that of air and the flexible substrate. ARCs such as  $MgF_2$  and  $LiF$  have been proven to be effective solutions in reducing reflection losses at the device/air interface. Coatings that give



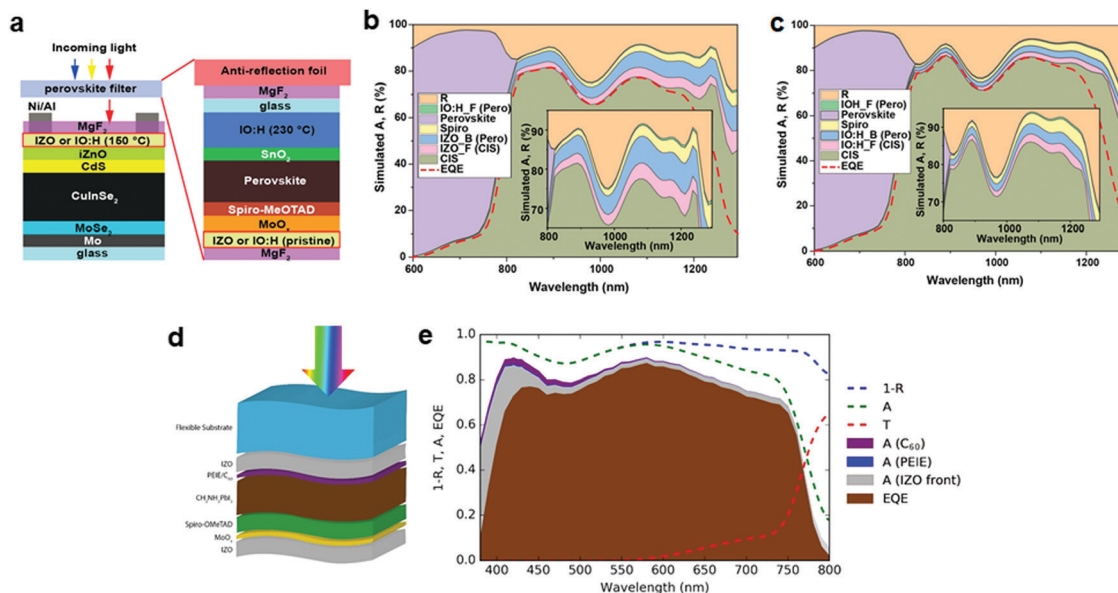


**Fig. 9** Optical loss analysis. (a) Schematic diagram of the 4-T perovskite/CIS tandems with IZO or IO:H electrodes. Absorptance loss analysis of the 4-T perovskite/CIS tandems (b) using IZO and (c) using IO:H as the back electrode of PSC and the front electrode of CIS. (d) Schematic drawing of the flexible NIR transparent PSC and (e) the optical loss analysis. (a–c) Reproduced with permission.<sup>62</sup> Copyright 2020, the American Chemical Society. (d and e) Reproduced with permission.<sup>37</sup> Copyright 2018, Springer Nature.

very low reflection over a broadband of frequencies can also be realized by the construction of multi-layer interference. (II) Application of polymer-based light management foils. Because of the retroreflective effect, these foils minimize reflection in a relatively wide wavelength range.<sup>104</sup>

## 6. Outlook

In the last years, the significant progress in flexible electronic and portable devices has resulted in an unprecedented demand for light-weight and flexible PV devices. Several technology breakthroughs have been realized in both 4-T and 2-T perovskite-based tandem solar cells, leading to tandem PCEs surpassing single-junction flexible PV technologies. Perovskite-based flexible tandem solar cells are very likely to be the next-generation flexible photovoltaic technology. On the other hand, development of perovskite-based tandems is still at an early stage. According to the technology maturity estimation methods, *e.g.*, technology readiness levels (TRLs), developed at the National Aeronautics and Space Administration (NASA) and modified by the European Commission (EC), flexible perovskite tandem solar cells are at a level of TRL1 and TRL2 (basic technology research). The next breakthrough in flexible perovskite tandems is to manufacture proof-of-concept demonstrators (TRL3) and validate them in independent laboratories (TRL4). So far, several main challenges lie ahead, hindering the advancement in flexible perovskite tandem solar cells. These challenges include maintaining high efficiency over large area devices, reduction of the environmental impact, and demonstration of the long-term operational stability. In the next, we provide insight into solving these challenges by

development of large-area low-temperature manufacturing processes and encapsulation methods.

### 6.1 Large area low-temperature manufacturing

Although high-efficiency flexible perovskite tandem solar cells have been demonstrated, these devices have so far been achieved with relatively small active areas (<1 cm<sup>2</sup>). Flexible perovskite tandem mini-module (200–800 cm<sup>2</sup>) or modules (>800 cm<sup>2</sup>) have not been reported yet. Increasing the cell area to the mini-module or module level usually results in efficiency loss because of increased series resistance, dead areas at the interconnection region and more shunting paths. While resistive and dead area losses can be largely mitigated by using highly conductive and transparent electrodes and rational design of P1, P2 and P3 patterning, reducing shunting loss relies on the development of deposition methods for every layer in perovskite tandem solar cells with high uniformity and without pinholes. Many low-temperature vapor and solution-based methods that have been successfully demonstrated in rigid perovskite tandem solar cells can be used for processing flexible perovskite tandem solar cells. These methods include magnetron sputtering,<sup>105,106</sup> hybrid chemical vapor deposition,<sup>107–111</sup> atomic layer deposition,<sup>32</sup> blade coating,<sup>112</sup> slot-die coating,<sup>113,114</sup> spray coating<sup>115,116</sup> and inkjet printing, *etc.*<sup>117</sup>

Several issues have to be considered when transferring the technology from rigid to flexible substrates. First, coefficient of thermal expansion (CTE) of flexible foil is several times and up to over a magnitude higher than the rigid substrate. Deposition recipes that result in uniform thin-film coating on rigid substrates may not work for flexible substrates (*i.e.*, forming cracks in thin film). Post-annealing temperature and ramp up/down speeds might need to be reoptimized. Second, surface roughness of



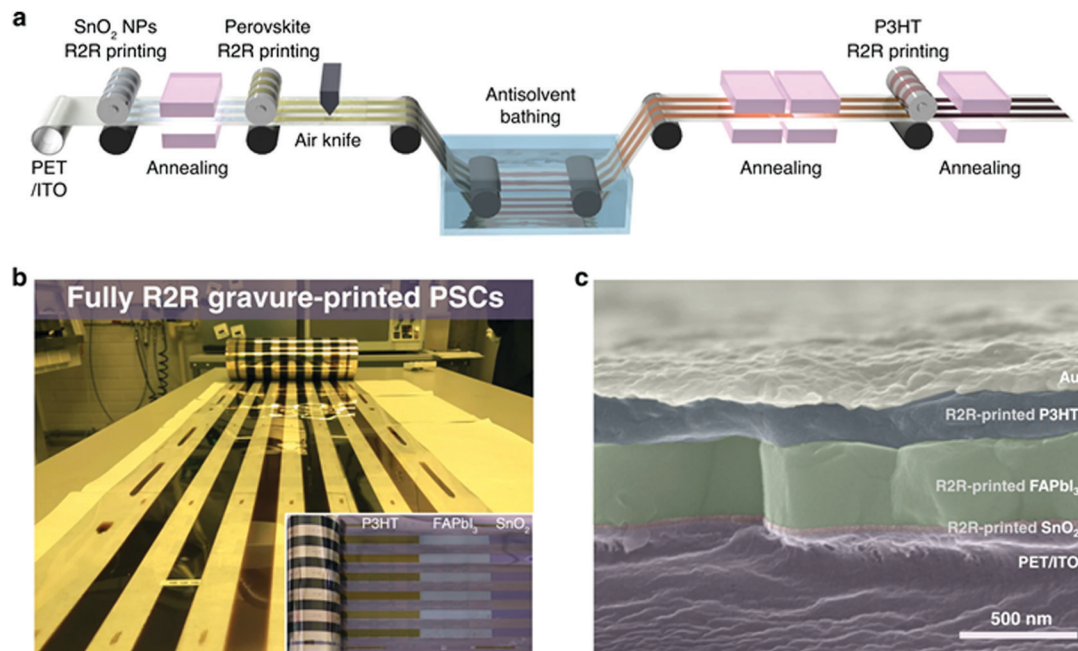


Fig. 10 Roll-to-roll manufacturing. (a) Schematic diagram of the R2R processing for flexible PSCs. (b) Photograph of R2R gravure-printed PSCs. Inset is a photograph of the R2R-processed roll showing constituent layers. (c) Cross-section SEM image of the flexible PSC. (a–c) Reproduced with permission.<sup>119</sup> Copyright 2020, Springer Nature.

flexible substrates is usually higher than rigid ones. The thickness of functional layers may need to be finely adjusted. A demonstration of flexible tandem mini-modules processed by these

low-temperature methods could be an encouraging step forward. These deposition recipes can be used as benchmarks for further optimization to obtain large-area flexible tandem modules.

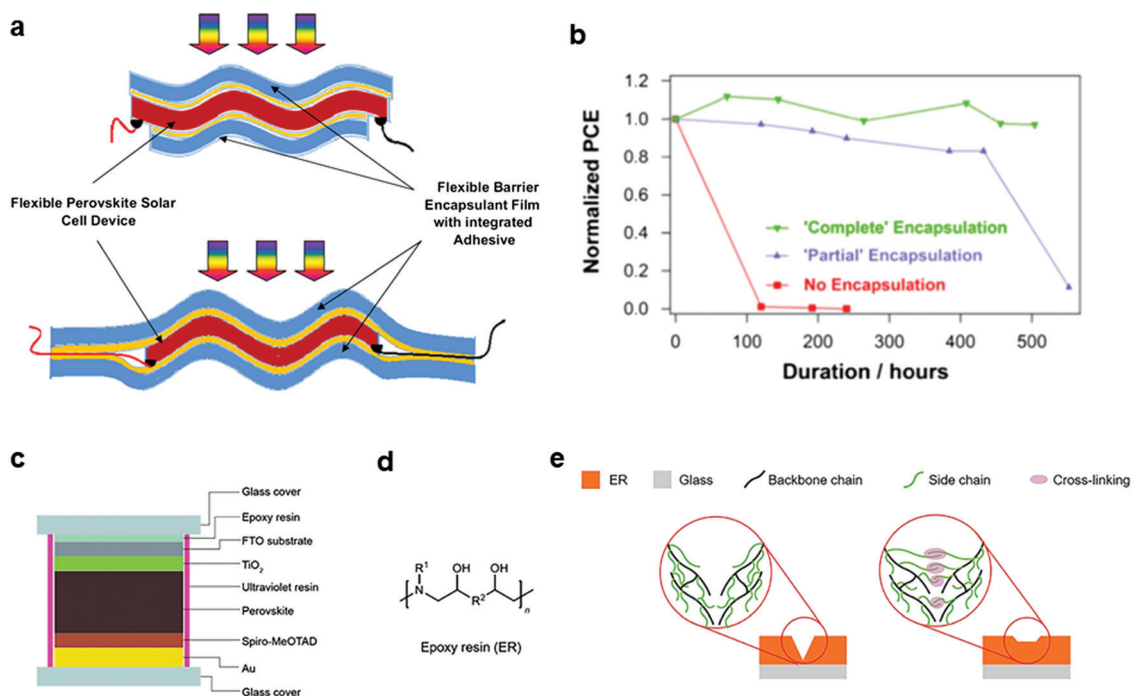


Fig. 11 Encapsulation against instability and Pb leakage. (a) Schematic diagram showing a partially (top) and a completely (bottom) encapsulated flexible PSC. (b) Stability of the flexible PSCs. The devices were kept in an ambient atmosphere. (c) Encapsulation methods against Pb leakage. (d) Molecular structure of the epoxy resin. (e) Schematic diagram showing the self-healing property of the epoxy resin. (a and b) Reproduced with permission.<sup>120</sup> Copyright 2015, Elsevier Inc. (c–e) Reproduced with permission.<sup>121</sup> Copyright 2019, Springer Nature.



In addition, the high flexibility makes roll-to-roll (R2R) methods especially suitable for manufacturing flexible perovskite tandem solar cells with high throughput and therefore low EPBT. In 2018, Dou *et al.* developed a perovskite precursor ink (methylamine-charged acetonitrile) that allows for fast ( $\sim 1$  s) perovskite crystallization and uniaxially oriented perovskite crystal growth. They demonstrated a uniformly R2R-coated perovskite absorber on a flexible glass substrate ( $25\text{ cm} \times 20\text{ m}$ ) with a PCE reaching 14.1% on  $0.15\text{ cm}^2$ .<sup>118</sup> In 2020, Kim *et al.* combined the R2R gravure-printing and anti-solvent bathing methods to fabricate flexible PSCs on PET substrates (Fig. 10a).<sup>119</sup> The SnO<sub>2</sub>, ETL, perovskite layer and the P3HT HTL are all R2R-processed at fast speeds ( $3\text{--}8\text{ m min}^{-1}$ ) (Fig. 10b). The flexible PSC shows a structure of PET/ITO/SnO<sub>2</sub>/FAPbI<sub>3</sub>/P3HT/Au (Fig. 10c). They demonstrated a pilot-scale (100 m long roll) flexible PSCs with an efficiency of 13.8% on an area of  $0.096\text{ cm}^2$ . These methods pave the way for large area and low-temperature manufacturing of flexible perovskite tandem mini-modules and modules.

## 6.2 Encapsulation for flexible perovskite tandems

Perovskite-based solar cells tend to degrade under external stresses such as moisture, heat, oxygen, illumination and vacuum, *etc.*<sup>11</sup> Instability of perovskite subcells is the Achilles heel hindering the long-term operational stability of the perovskite-based flexible tandems. Realization of stable perovskite-based flexible tandems relies on breakthroughs from the perovskite cell side, instead of the partner cell. In addition, high-efficiency PSCs contain ionic Pb<sup>2+</sup> in the absorber, accounting for around 30% of the weight of the perovskite absorber. Potential environmental impacts entailed by perovskite-based solar cells remain a significant concern. The good news is that recent advances on encapsulation methods for PSCs may hold the key to these issues for flexible perovskite tandems.

Weerasinghe *et al.* investigated the effect of various encapsulation methods on the stability of the flexible PSCs.<sup>120</sup> They used a plastic barrier encapsulant, *i.e.*, Viewbarriers (Mitsubishi Plastic, Inc) to partially or completely laminate the flexible PSCs (Fig. 11a) and kept the flexible PSCs under ambient conditions. The encapsulated devices show substantially improved shell-lifetime compared with the non-encapsulated devices (Fig. 11b). The partially encapsulated devices displayed a slow PCE decay at the first 450 h and a drastic decay afterward, and the completely encapsulated device maintains the initial PCE after 500 h.

Jiang *et al.* quantitatively estimated the Pb leakage from damaged perovskite solar modules with a structure shown in Fig. 11c.<sup>121</sup> Experimental and simulation results suggest that the microcracks formed during external impact are a crucial factor determining the Pb leakage rates. They developed an epoxy resin encapsulation method that reduced the Pb leakage rate by a factor of 375 compared to the normal encapsulation method. Li *et al.*, deposited transparent and lead-absorbing materials on both sides of the devices that can chemically absorb leaked Pb of up to 96%.<sup>122</sup> Chen *et al.* reported an abundant, low-cost and chemically robust cation-exchange

resin (CER)-based encapsulation approach that exhibits both high adsorption capacity and high adsorption rate of lead in water, and negligible effect on the solar cell efficiency.<sup>123</sup> Although these encapsulation methods are demonstrated on rigid PSCs, with some modifications they can very likely be implemented in flexible perovskite tandems.

Aiming at the development of stable and low environmental impact flexible perovskite tandem solar cells, encapsulation materials should process the following criteria, including high flexibility, low WATR and OTR, high optical transparency and low reflectivity, high mechanical robustness and the capability to stabilize the leaked Pb<sup>2+</sup>. In addition, suitable thin-film fabrication methods have to be developed for these advanced encapsulation materials.

## Conflicts of interest

There are no conflicts of interest to declare.

## Acknowledgements

Y. J. acknowledges the funding support from the Energy Materials and Optoelectronics Unit of Songshan Lake Materials Laboratory. Y. B. Q. acknowledges the funding support from the Energy Materials and Surface Sciences Unit of the Okinawa Institute of Science and Technology Graduate University.

## References

- 1 Future of Photovoltaic (International Renewable Energy Agency, 2019) [https://www.irena.org/-/media/Files/IRENA/Agency/Publication/2019/Nov/IRENA\\_Future\\_of\\_Solar\\_PV\\_2019.pdf](https://www.irena.org/-/media/Files/IRENA/Agency/Publication/2019/Nov/IRENA_Future_of_Solar_PV_2019.pdf).
- 2 Customized solar panels & films (Flisom, accessed: 2021) <https://www.flisom.com/industries-customized-solar-panels-films/>.
- 3 Best wearable solar energy generating system (Ecofriend, accessed: 2021) <https://ecofriend.com/wearable-solar-energy-generating-systems.html>.
- 4 Flexible Solar Cells Could Release Toxic Metals After Disposal (Chemical and Engineering News, 2013) <https://cen.acs.org/articles/91/web/2013/10/Flexible-Solar-Cells-Release-Toxic.html>.
- 5 O. Malinkiewicz, M. Imaizumi, S. B. Sapkota, T. Ohshima and S. Öz, Radiation effects on the performance of flexible perovskite solar cells for space applications, *Emergent Mater.*, 2020, **3**, 9–14.
- 6 Flexing our solar muscle: solar for everyone, everywhere (CSIRO, 2019) <https://blog.csiro.au/flexing-our-solar-muscle-solar-for-everyone-everywhere/>.
- 7 M. Kaltenbrunner, G. Adam, E. D. Glowacki, M. Drack, R. Schwödauer, L. Leonat, D. H. Apaydin, H. Groiss, M. C. Scharber, M. S. White, N. S. Sariciftci and S. Bauer, Flexible high power-per-weight perovskite solar cells with



- chromium oxide–metal contacts for improved stability in air, *Nat. Mater.*, 2015, **14**, 1032–1039.
- 8 Smartphones (Samsung, Accessed: 2021) [https://www.samsung.com/hk\\_en/](https://www.samsung.com/hk_en/).
  - 9 Phones (Huawei, Accessed: 2021) <https://www.huawei.com/en/>.
  - 10 Solar electric propulsion (NASA, 2020) [www.nasa.gov/mision\\_pages/tdm/sep/index.html](http://www.nasa.gov/mision_pages/tdm/sep/index.html).
  - 11 Y. Jiang, S.-C. Yang, Q. Jeangros, S. Pisoni, T. Moser, S. Buecheler, A. N. Tiwari and F. Fu, Mitigation of Vacuum and Illumination-Induced Degradation in Perovskite Solar Cells by Structure Engineering, *Joule*, 2020, **4**, 1–17.
  - 12 Flexible Solar Cell Market Size, Share, Growth 2021, by Global Top Companies, Trends by Types and Application, Forecast to 2023 (Market Reports world, 2021) <https://www.marketreportsworld.com/thankyou/request-sample/13117464>.
  - 13 J. Ramanujam, D. M. Bishop, T. K. Todorov, O. Gunawan, J. Rath, R. Nekovei, E. Artegiani and A. Romeo, Flexible CIGS, CdTe and a-Si:H based thin film solar cells: A review, *Prog. Mater. Sci.*, 2020, **100**, 100619.
  - 14 B. M. Basol, V. K. Kapur, A. Halani and C. Leidholm, Copper indium diselenide thin-film solar-cells fabricated on flexible foil substrates, *Sol. Energy Mater. Sol. Cells*, 1993, **29**, 163–173.
  - 15 B. M. Basol, C. K. Kapur, C. R. Leidholm and A. Halani, Flexible and light weight copper indium diselenide solar cells on polyimide substrates, Photovoltaic Specialists Conference, 1996., Conference Record of the Twenty Fifth IEEE, 1996.
  - 16 T. Yagioka and T. Nakada, Cd-Free Flexible Cu(In,Ga)Se<sub>2</sub> Thin Film Solar Cells with ZnS(O,H) Buffer Layers on Ti Foils, *Appl. Phys. Express*, 2009, **2**, 072201.
  - 17 A. Chirilă, S. Buecheler, F. Pianezzi, P. Bloesch, C. Gretener, A. R. Uhl, C. Fella, L. Kranz, J. Perrenoud, S. Seyrling, R. Verma, S. Nishiwaki, Y. E. Romanyuk, G. Bilger and A. N. Tiwari, Highly efficient Cu(In,Ga)Se<sub>2</sub> solar cells grown on flexible polymer films, *Nat. Mater.*, 2011, **10**, 857–861.
  - 18 A. Chirilă, P. Reinhard, F. Pianezzi, P. Bloesch, A. R. Uhl, C. Fella, L. Kranz, D. Keller, C. Gretener, H. Hagendorfer, D. Jaeger, R. Erni, S. Nishiwaki, S. Buecheler and A. N. Tiwari, Potassium-induced surface modification of Cu(In,Ga)Se<sub>2</sub> thin films for high-efficiency solar cells, *Nat. Mater.*, 2013, **12**, 1107–1111.
  - 19 R. Carron, S. Nishiwaki, T. Feurer, R. Hertwig, E. Avancini, J. Löckinger, S.-C. Yang, S. Buecheler and A. N. Tiwari, Advanced Alkali Treatments for High-Efficiency Cu(In,Ga)Se<sub>2</sub> Solar Cells on Flexible Substrates, *Adv. Energy Mater.*, 2019, **9**, 1900408.
  - 20 M. A. Contreras, B. Egaas, K. Ramanathan, J. Hiltner, A. Swartzlander, F. Hasoon and R. Noufi, Progress toward 20% efficiency in Cu(In,Ga)Se<sub>2</sub> polycrystalline thin-film solar cells, *Prog. Photovoltaics*, 1999, **7**, 311–316.
  - 21 Product document (MiaSolé Hi-Tech Corp, Access: 2021) <http://miasole.com/>.
  - 22 J.-C. Wang, W. T. Weng, M.-Y. Tsai, M.-K. Lee, S.-F. Horng, T.-P. Perng, C.-C. Kei, C.-C. Yu and H.-F. Meng, Highly efficient flexible inverted organic solar cells using atomic layer deposited ZnO as electron selective layer, *J. Mater. Chem.*, 2010, **20**, 862–866.
  - 23 K. Yao, K.-K. Xin, C.-C. Chueh, K.-S. Chen, Y.-X. Xu and A. K.-Y. Jen, Enhanced Light-Harvesting by Integrating Synergistic Microcavity and Plasmonic Effects for High-Performance ITO-Free Flexible Polymer Solar Cells, *Adv. Funct. Mater.*, 2015, **28**, 567–574.
  - 24 Q. Liu, J. Toudert, L. Ciammaruchi, G. Martínez-Denegria and J. Martorell, High open-circuit voltage and short-circuit current flexible polymer solar cells using ternary blends and ultrathin Ag-based transparent electrodes, *J. Mater. Chem. A*, 2017, **5**, 25476–25484.
  - 25 T. Yan, W. Song, J. Huang, R. Peng, L. H. Huang and Z. Ge, 16.67% Rigid and 14.06% Flexible Organic Solar Cells Enabled by Ternary Heterojunction Strategy, *Adv. Mater.*, 2019, **31**, 1902210.
  - 26 A. Kojima, K. Teshima, Y. Shirai and T. Miyasaka, Organometal halide perovskites as visible-light sensitizers for photovoltaic cells, *J. Am. Chem. Soc.*, 2009, **131**, 6050–6051.
  - 27 L. Qiu, L. K. Ono and Y. B. Qi, Advances and challenges to the commercialization of organic–inorganic halide perovskite solar cell technology, *Mater. Today Energy*, 2018, **7**, 169–189.
  - 28 C. Wang, L. Guan, D. Zhao, Y. Yu, C. R. Grice, Z. Song, R. A. Awni, J. Chen, J. Wang, X. Zhao and Y. Yan, Water Vapor Treatment of Low-Temperature Deposited SnO<sub>2</sub> Electron Selective Layers for Efficient Flexible Perovskite Solar Cells, *ACS Energy Lett.*, 2017, **2**, 2118–2124.
  - 29 M. H. Kumar, N. Yantara, S. Dharani, M. Graetzel, S. Mhaisalkar, P. P. Boix and N. Mathews, Flexible, low-temperature, solution processed ZnO-based perovskite solid state solar cells, *Chem. Commun.*, 2013, **49**, 11089–11091.
  - 30 J. Yoon, H. Sung, G. Lee, W. Cho, N. Ahn, H. S. Jung and M. Choi, Superflexible, high-efficiency perovskite solar cells utilizing graphene electrodes: towards future foldable power sources, *Energy Environ. Sci.*, 2017, **10**, 337–345.
  - 31 K. Huang, Y. Peng, Y. Gao, J. Shi, H. Li, X. Mo, H. Huang, Y. Gao, L. Ding and J. Yang, High-Performance Flexible Perovskite Solar Cells via Precise Control of Electron Transport Layer, *Adv. Energy Mater.*, 2019, **9**, 1901419.
  - 32 D. Liu and T. L. Kelly, Perovskite solar cells with a planar heterojunction structure prepared using room-temperature solution processing techniques, *Nat. Photonics*, 2013, **8**, 133–138.
  - 33 S. S. Shin, W. S. Yang, J. H. Noh, J. H. Suk, N. J. Jeon, J. H. Park, J. S. Kim, W. M. Seong and S. S. I. High-performance, flexible perovskite solar cells exploiting Zn<sub>2</sub>SnO<sub>4</sub> prepared in solution below 100 °C, *Nat. Commun.*, 2015, **6**, 7410.
  - 34 D. Yang, R. Yang, X. Ren, X. Zhu, Z. Yang, C. Li and S. Liu, Hysteresis-Suppressed High-Efficiency Flexible Perovskite Solar Cells Using Solid-State Ionic-Liquids for Effective Electron Transport, *Adv. Mater.*, 2016, **28**, 5206–5213.
  - 35 A. F. Palmstrom, G. E. Eperon, T. Leijtens, R. Prasanna, S. N. Habisreutinger, W. Nemeth, E. A. Gaubing,



- S. P. Dunfield, M. Reese, S. Nanayakkara, T. Moot, J. Werner, J. Liu, B. To, S. T. Christensen, M. McGehee, F. A. M. van Hest, J. M. Luther, J. J. Berry and D. T. Moore, Enabling Flexible All-Perovskite Tandem Solar Cells, *Joule*, 2019, 3, 2193–2204.
- 36 S. Pisoni, F. Fu, T. Feurer, M. Makha, B. Bissig, S. Nishiwaki, A. N. Tiwari and S. Buecheler, Flexible NIR-transparent perovskite solar cells for all-thin-film tandem photovoltaic devices, *J. Mater. Chem. A*, 2017, 5, 13639–13647.
- 37 S. Pisoni, R. Carron, T. Moser, T. Feurer, F. Fu, S. Nishiwaki, A. N. Tiwari and S. Buecheler, Tailored lead iodide growth for efficient flexible perovskite solar cells and thin-film tandem devices, *NPG Asia Mater.*, 2018, 10, 1076–1085.
- 38 Record breaking 23% efficiency proved for flexible perovskite/CIGS-tandem (Solliance, 2020) <http://miasole.com/record-breaking-23-efficiency-proved-for-flexible-perovskite-cigs-tandem/>.
- 39 F. Fu, S. Nishiwaki, J. Werner, T. Feurer, S. Pisoni, Q. Jeangros, S. Buecheler, C. Ballif and A. N. Tiwari, Flexible perovskite/Cu(In,Ga)Se<sub>2</sub> monolithic tandem solar cells, arXiv:1907.10330, 2019.
- 40 Z. Li, S. Wu, J. Zhang, K. C. Lee, H. Lei, F. Lin, Z. Wang, Z. Zhu and A. K. Y. Jen, Hybrid Perovskite-Organic Flexible Tandem Solar Cell Enabling Highly Efficient Electrocatalysis Overall Water Splitting, *Adv. Energy Mater.*, 2020, 10, 2000361.
- 41 C. Wang, Z. Song, C. Li, D. Zhao and Y. Yan, Low-Bandgap Mixed Tin-Lead Perovskites and Their Applications in All-Perovskite Tandem Solar Cells, *Adv. Funct. Mater.*, 2019, 29, 1808801.
- 42 H. Shen, T. Duong, J. Peng, D. Jacobs, N. Wu, J. Gong, Y. Wu, S. K. Karuturi, X. Fu, K. Weber, X. Xiao, T. P. White and K. Catchpole, Mechanically-stacked perovskite/CIGS tandem solar cells with efficiency of 23.9% and reduced oxygen sensitivity, *Energy Environ. Sci.*, 2018, 11, 394–406.
- 43 R. K. Kothandaraman, Y. Jiang, T. Feurer, A. N. Tiwari and F. Fu, Near-Infrared-Transparent Perovskite Solar Cells and Perovskite-Based Tandem Photovoltaics, *Small Methods*, 2020, 4, 2000395.
- 44 M. D. Bastiani, A. J. Mirabelli, Y. Hou, F. Gota, E. Aydin, T. G. Allen, J. Troughton, A. S. Subbiah, F. H. Isikgor, J. Liu, L. Xu, B. Chen, E. V. Kerschaver, D. Baran, B. Fraboni, M. F. Salvador, U. W. Paetzold, E. H. Sargent and S. D. Wolf, Efficient bifacial monolithic perovskite/silicon tandem solar cells *via* bandgap engineering, *Nat. Energy*, 2021, 6, 167–175.
- 45 J. Gong, S. B. Darling and F. You, Perovskite photovoltaics: life-cycle assessment of energy and environmental impacts, *Energy Environ. Sci.*, 2015, 8, 1953–1968.
- 46 PV FAQs (U.S. Department of Energy, Accessed: 2021) <https://www.nrel.gov/docs/fy04osti/35489.pdf>.
- 47 I. Celik, A. B. Phillips, Z. Song, Y. Yan, R. J. Ellingson, M. J. Heben and D. Apul, Energy Payback Time (EPBT) and Energy Return on Energy Invested (EROI) of Perovskite Tandem Photovoltaic Solar Cells, *IEEE J. Photovoltaics*, 2018, 8, 305–309.
- 48 I. Celik, A. B. Phillips, Z. Song, Y. Yan, R. J. Ellingson, M. J. Heben and D. Apul, Environmental analysis of perovskites and other relevant solar cell technologies in a tandem configuration, *Energy Environ. Sci.*, 2017, 10, 1874–1884.
- 49 V. Muteri, M. Cellura, D. Curto, V. Franzitta, S. Longo, M. Mistretta and M. L. Parisi, Review on Life Cycle Assessment of Solar Photovoltaic Panels, *Energies*, 2020, 13, 252.
- 50 S. A. Hashemi, S. Ramakrishna and A. G. Aberle, Recent progress in flexible-wearable solar cells for self-powered electronic devices, *Energy Environ. Sci.*, 2020, 13, 685–743.
- 51 J. Zhang, W. Zhang, H.-M. Cheng and S. R. P. Silva, Critical review of recent progress of flexible perovskite solar cells, *Mater. Today*, 2020, 39, 66–88.
- 52 B. Dou, E. M. Miller, J. A. Christians, E. M. Sanehira, T. R. Klein, F. S. Barnes, S. E. Shaheen, S. M. Garner, S. Ghosh, A. Mallick, D. Basak and M. F. A. M. v. Hest, High-Performance Flexible Perovskite Solar Cells on Ultrathin Glass: Implications of the TCO, *J. Phys. Chem. Lett.*, 2017, 8, 4960–4966.
- 53 Z. Liu, L. Qiu, L. K. Ono, S. He, Z. Hu, M. Jiang, G. Tong, Z. Wu, Y. Jiang, D.-Y. Son, Y. Dang, S. Kazaoui and Y. B. Qi, A holistic approach to interface stabilization for efficient perovskite solar modules with over 2000-hour operational stability, *Nat. Energy*, 2020, 5, 596–604.
- 54 H. Wang, Y. Zhao, Z. Wang, Y. Liu, Z. Zhao, G. Xu, T.-H. Han, C. Chen, D. Bao, Y. Huang, Y. Duan and Y. Yang, Hermetic seal for perovskite solar cells: An improved plasma enhanced atomic layer deposition encapsulation, *Nano Energy*, 2020, 69, 104375.
- 55 R. Cheacharoen, N. Rolston, D. Harwood, K. A. Bush, R. H. Dauskardt and M. D. McGehee, Design and understanding of encapsulated perovskite solar cells to withstand temperature cycling, *Energy Environ. Sci.*, 2018, 11, 144–150.
- 56 S. Ma, Y. Bai, H. Wang, H. Zai, J. Wu, L. Li, S. Xiang, N. Liu, L. Liu, C. Zhu, G. Liu, X. Niu, H. Chen, H. Zhou, Y. Li and Q. Chen, 1000 h Operational Lifetime Perovskite Solar Cells by Ambient Melting Encapsulation, *Adv. Energy Mater.*, 2020, 10, 1902472.
- 57 S. Wang, Y. Jiang, E. J. Juarez-Perez, L. K. Ono and Y. B. Qi, Accelerated degradation of methylammonium lead iodide perovskites induced by exposure to iodine vapour, *Nat. Energy*, 2016, 2, 16195.
- 58 E. J. Juarez-Perez, Z. Hawash, S. R. Raga, L. K. Ono and Y. B. Qi, Thermal degradation of CH<sub>3</sub>NH<sub>3</sub>PbI<sub>3</sub> perovskite into NH<sub>3</sub> and CH<sub>3</sub>I gases observed by coupled thermogravimetry–mass spectrometry analysis, *Energy Environ. Sci.*, 2016, 9, 3406–3410.
- 59 E. J. Juarez-Perez, L. K. Ono, M. Maeda, Y. Jiang, Z. Hawash and Y. B. Qi, Photodecomposition and thermal decomposition in methylammonium halide lead perovskites and inferred design principles to increase photovoltaic device stability, *J. Mater. Chem. A*, 2018, 6, 9604–9612.



- 60 Corning Willow Glass Lamination (Corning Inc., Accessed: 2021) <https://www.corning.com/worldwide/en/innovation/corning-emerging-innovations/corning-willow-glass.html>.
- 61 Y. Yee Kee, S. S. Tan, T. K. Yong, C. H. Nee, S. S. Yap, T. Y. Tou, G. S. Z. E. Horvath, J. P. Moscatello and Y. K. Yap, Low-temperature synthesis of indium tin oxide nanowires as the transparent electrodes for organic light emitting devices, *Nanotechnology*, 2012, **23**, 025706.
- 62 Y. Jiang, T. Feurer, R. Carron, G. Torres Sevilla, T. Moser, S. Pisoni, R. Erni, M. D. Rossell, M. Ochoa, R. Hertwig, A. N. Tiwari and F. Fu, High-Mobility  $\text{In}_2\text{O}_3\text{:H}$  Electrodes for Four-Terminal Perovskite/CuInSe<sub>2</sub> Tandem Solar Cells, *ACS Nano*, 2020, 7502–7512.
- 63 X. Hu, X. Meng, L. Zhang, Y. Zhang, Z. Cai, Z. Huang, M. Su, Y. Wang, M. Li, F. Li, X. Yao, F. Wang, W. Ma, Y. Chen and Y. Song, A Mechanically Robust Conducting Polymer Network Electrode for Efficient Flexible Perovskite Solar Cells, *Joule*, 2019, **3**, 1–14.
- 64 Y. Li, L. Meng, Y. M. Yang, Z. H. G. Xu, Q. Chen, J. You, G. Li, Y. Yang and Y. Li, High-efficiency robust perovskite solar cells on ultrathin flexible substrates, *Nat. Commun.*, 2016, **7**, 10214.
- 65 X. Xie, C. Wu, S. Sun, X. Xu, W. Xu, G. Qin and L. Xiao, Semitransparent Perovskite Solar Cells with Dielectric/Metal/Dielectric Top Electrodes, *Energy Technol.*, 2020, **8**, 1900868.
- 66 I. Jeon, T. Chiba, C. Delacou, Y. Guo, A. Kaskela, O. Reynaud, E. I. Kauppinen, S. Maruyama and Y. Matsuo, Single walled carbon nanotube film as electrode in indium-free planar heterojunction perovskite solar cells: investigation of electron-blocking layers and dopants, *Nano Lett.*, 2015, **15**, 6665–6671.
- 67 N. N. Lal, Y. Dkhissi, W. Li, Q. Hou, Y.-B. Cheng and U. Bach, Perovskite Tandem Solar Cells, *Adv. Energy Mater.*, 2017, **7**, 1602761.
- 68 C. O. R. Quiroz, Y. Shen, M. Salvador, K. Forberich, N. Schrenker, G. D. Spyropoulos, T. Heumüller, B. Wilkinson, T. Kirchartz, E. Spiecker, P. J. Verlinden, X. Zhang, M. A. Green, A. Ho-Baillie and C. J. Brabec, Balancing electrical and optical losses for efficient 4-terminal Si-perovskite solar cells with solution processed percolation electrodes, *J. Mater. Chem. A*, 2018, **6**, 3583–3592.
- 69 Perovskite and CIGS tandem solar cell reaches 21.5% conversion efficiency (Solliance, 2019) <https://www.solarpowerworldonline.com/2019/01/perovskite-and-cigs-tandem-solar-cell-reaches-21-5-conversion-efficiency/>.
- 70 S. Li, C. Wang, D. Zhao, Y. An, Y. Zhao, X. Zhao and X. Li, Flexible semitransparent perovskite solar cells with gradient energy levels enable efficient tandems with  $\text{Cu}(\text{In,Ga})\text{Se}_2$ , *Nano Energy*, 2020, **78**, 105378.
- 71 Y. Zhang, Z. Wu, P. Li, L. K. Ono, Y. B. Qi, J. Zhou, H. Shen, C. Surya and Z. Zheng, Fully Solution-Processed TCO-Free Semitransparent Perovskite Solar Cells for Tandem and Flexible Applications, *Adv. Energy Mater.*, 2018, **8**, 1701569.
- 72 C. W. Jang, J. M. Kim and S.-H. Choi, Lamination-produced semi-transparent/flexible perovskite solar cells with doped-graphene anode and cathode, *J. Alloys Compd.*, 2019, **775**, 905–911.
- 73 C. C. Stoumpos, C. D. Malliakas and M. G. Kanatzidis, Semiconducting Tin and Lead Iodide Perovskites with Organic Cations: Phase Transitions, High Mobilities, and Near-Infrared Photoluminescent Properties, *Inorg. Chem.*, 2013, **15**, 9019–9038.
- 74 N. K. Noel, S. D. Stranks, A. Abate, C. Wehrenfennig, S. Guarnera, A.-A. Haghighirad, A. Sadhanala, G. E. Eperon, S. K. Pathak, M. B. Johnston, A. Petrozza, L. M. Herza and H. J. Snaith, Lead-free organic-inorganic tin halide perovskites for photovoltaic applications, *Energy Environ. Sci.*, 2014, **7**, 3061–3068.
- 75 S. A. A. Shah, M. H. Sayyad, K. Khan, K. Guo, F. Shen, J. Sun, A. K. Tareen, Y. Gong and Z. Guo, Progress towards High-Efficiency and Stable Tin-Based Perovskite Solar Cells, *Energies*, 2020, **13**, 5092.
- 76 H. Hoshi, N. Shigeeda and T. Dai, Improved oxidation stability of tin iodide cubic perovskite treated by 5-ammonium valeric acid iodide, *Mater. Lett.*, 2016, **183**, 391–393.
- 77 T. Handa, T. Yamada, H. Kubota, S. Ise, Y. Miyamoto and Y. Kanemitsu, Photocarrier Recombination and Injection Dynamics in Long-Term Stable Lead-Free  $\text{CH}_3\text{NH}_3\text{SnI}_3$  Perovskite Thin Films and Solar Cells, *J. Phys. Chem. C*, 2017, **131**, 16158–16165.
- 78 P. Wang, F. Li, K. Jiang, Y. Zhang, H. Fan, Y. Zhang, Y. Miao, J.-H. Huang, C. Gao, X. Zhou, F. Wang, L.-M. Yang, C. Zhan and Y. Song, Ion Exchange/Insertion Reactions for Fabrication of Efficient Methylammonium Tin Iodide Perovskite Solar Cells, *Adv. Sci.*, 2020, **7**, 1903047.
- 79 T. Wu, X. Liu, X. He, Y. Wang, X. Meng, T. Noda, X. Yang and L. Han, Efficient and stable tin-based perovskite solar cells by introducing  $\pi$ -conjugated Lewis base, *Sci. China Chem.*, 2020, **63**, 107–115.
- 80 J. Xi, Z. Wu, B. Jiao, H. Dong, C. Ran, C. Piao, T. Lei, T.-B. Song, W. Ke, T. Yokoyama, X. Hou and M. G. Kanatzidis, Multichannel Interdiffusion Driven  $\text{FASnI}_3$  Film Formation Using Aqueous Hybrid Salt/Polymer Solutions toward Flexible Lead-Free Perovskite Solar Cells, *Adv. Mater.*, 2017, **29**, 1606964.
- 81 J. Im, C. C. Stoumpos, H. Jin, A. J. Freeman and M. G. Kanatzidis, Antagonism between Spin-Orbit Coupling and Steric Effects Causes Anomalous Band Gap Evolution in the Perovskite Photovoltaic Materials  $\text{CH}_3\text{NH}_3\text{Sn}_{1-x}\text{Pb}_x\text{I}_3$ , *J. Phys. Chem. Lett.*, 2015, **6**, 3503–3509.
- 82 A. Goyal, S. McKechnie, D. Pashov, W. Tumas, M. van Schilfhaarde and V. Stevanović, Origin of Pronounced Nonlinear Band Gap Behavior in Lead-Tin Hybrid Perovskite Alloys, *Chem. Mater.*, 2018, **11**, 3920–3928.
- 83 S. Gu, R. Lin, Q. Han, Y. Gao, H. Tan and J. Zhu, Tin and Mixed Lead-Tin Halide Perovskite Solar Cells: Progress and their Application in Tandem Solar Cells, *Adv. Mater.*, 2020, **32**, 1907392.



- 84 H. Chen, Z. Peng, K. Xu, Q. Wei, D. Yu, C. Han, H. Li and Z. Ning, Band alignment towards high-efficiency NiOx-based Sn–Pb mixed perovskite solar cells, *Sci. China Mater.*, 2021, **64**, 537–546.
- 85 F. Zuo, S. T. Williams, P.-W. Liang, C.-C. Chueh, C.-Y. Liao and A. K.-Y. Jen, Binary-Metal Perovskites Toward High-Performance Planar-Heterojunction Hybrid Solar Cells, *Adv. Mater.*, 2014, **26**, 6454–6460.
- 86 D. Zhao, Y. Yu, C. Wang, W. Liao, N. Shrestha, C. R. Grice, A. J. Cimaroli, L. Guan, R. J. Ellingson, K. Zhu, X. Zhao, R.-G. Xiong and Y. Yan, Low-bandgap mixed tin–lead iodide perovskite absorbers with long carrier lifetimes for all-perovskite tandem solar cells, *Nat. Energy*, 2017, **2**, 17018.
- 87 D. Zhao, C. Chen, C. Wang, M. M. Junda, Z. Song, C. R. Grice, Y. Yu, C. Li, B. Subedi, N. J. Podraza, X. Zhao, G. Fang, R.-G. Xiong, K. Zhu and Y. Yan, Efficient two-terminal all-perovskite tandem solar cells enabled by high-quality low-bandgap absorber layers, *Nat. Energy*, 2018, **3**, 1093–1100.
- 88 J. Tong, Z. Song, D. H. Kim, X. Chen, C. Chen, A. F. Palmstrom, P. F. Ndione, M. O. Reese, S. P. Dunfield, O. G. Reid, J. Liu, F. Zhang, S. P. Harvey, Z. Li, S. T. Christensen, G. Teeter, D. Zhao, M. M. Al-Jassim, M. F. A. M. van Hest, M. C. Beard, S. E. Shaheen, J. J. Berry, Y. Yan and K. Zhu, Carrier lifetimes of > 1 ms in Sn–Pb perovskites enable efficient all-perovskite tandem solar cells, *Science*, 2019, **364**, 475–479.
- 89 R. Lin, K. Xiao, Z. Qin, Q. Han, C. Zhang, M. Wei, M. I. Saidaminov, Y. Gao, J. Xu, M. Xiao, A. Li, J. Zhu, E. H. Sargent and H. Tan, Monolithic all-perovskite tandem solar cells with 24.8% efficiency exploiting composition to suppress Sn(ii) oxidation in precursor ink, *Nat. Energy*, 2019, **4**, 864–873.
- 90 R. Prasanna, A. Gold-Parker, T. Leijtens, B. Conings, A. Babayigit, H.-G. Boyen, M. F. Toney and M. D. McGehee, Band Gap Tuning via Lattice Contraction and Octahedral Tilting in Perovskite Materials for Photovoltaics, *J. Am. Chem. Soc.*, 2017, **139**, 11117–11124.
- 91 Y. Jiang, X. Zhang, Q.-Q. Ge, B.-B. Yu, Y.-G. Zou, W.-J. Jiang, W.-G. Song, L.-J. Wan and J.-S. Hu, ITO@Cu<sub>2</sub>S Tunnel Junction Nanowire Arrays as Efficient Counter Electrode for Quantum-Dot-Sensitized Solar Cells, *Nano Lett.*, 2014, **14**, 365–372.
- 92 Y. Jiang, B.-B. Yu, J. Liu, Z.-H. Li, J.-K. Sun, X.-H. Zhong, J.-S. Hu, W.-G. Song and L.-J. Wan, Boosting the Open Circuit Voltage and Fill Factor of QDSSCs Using Hierarchically Assembled ITO@Cu<sub>2</sub>S Nanowire Array Counter Electrodes, *Nano Lett.*, 2015, **15**, 3088–3095.
- 93 M. D. Bastiani, A. S. Subbiah, E. Aydin, F. H. Isikgor, T. G. Allen and S. D. Wolf, Recombination junctions for efficient monolithic perovskite-based tandem solar cells: physical principles, properties, processing and prospects, *Mater. Horiz.*, 2020, **7**, 2791–2809.
- 94 K. Xiao, R. Lin, Q. Han, Y. Hou, Z. Qin, H. T. Nguyen, J. Wen, M. Wei, V. Yeddu, M. I. Saidaminov, Y. Gao, X. Luo, Y. Wang, H. Gao, C. Zhang, J. Xu, J. Zhu, E. H. Sargent and H. Tan, All-perovskite tandem solar cells with 24.2% certified efficiency and area over 1 cm<sup>2</sup> using surface-anchoring zwitterionic antioxidant, *Nat. Energy*, 2020, **5**, 870–880.
- 95 C. Li, Z. Song, C. Chen, C. Xiao, B. Subedi, S. P. Harvey, N. S. Shrestha, K. K. Subedi, L. Chen, D. Liu, Y. Li, Y.-W. Kim, C.-S. Jiang, M. J. Heben, D. Zhao, R. J. Ellingson, N. J. Podraza, M. Al-Jassim and Y. Yan, Low-bandgap mixed tin–lead iodide perovskites with reduced methylammonium for simultaneous enhancement of solar cell efficiency and stability, *Nat. Energy*, 2020, **5**, 768–776.
- 96 Z. Yu, Z. Yang, Z. Ni, Y. Shao, B. Chen, Y. Lin, H. Wei, Z. J. Yu, Z. Holman and J. Huang, Simplified interconnection structure based on C<sub>60</sub>/SnO<sub>2-x</sub> for all-perovskite tandem solar cells, *Nat. Energy*, 2020, **5**, 657–665.
- 97 M. Jošt, T. Bertram, D. Koushik, J. A. Marquez, M. A. Verheijen, M. D. Heinemann, E. Köhnen, A. Al-Ashouri, S. Braunger, F. Lang, B. Rech, T. Unold, M. Creatore, I. Laueremann, C. A. Kaufmann, R. Schlatmann and S. Albrecht, 21.6%-Efficient Monolithic Perovskite/Cu(In,Ga)Se<sub>2</sub> Tandem Solar Cells with Thin Conformal Hole Transport Layers for Integration on Rough Bottom Cell Surfaces, *ACS Energy Lett.*, 2019, **4**, 583–590.
- 98 Q. Han, Y.-T. Hsieh, L. Meng, J.-L. Wu, P. Sun, E.-P. Yao, S.-Y. Chang, S.-H. Bae, Y. Kato, V. Bermudez and Y. Yang, High-performance perovskite/Cu(In,Ga)Se<sub>2</sub> monolithic tandem solar cells, *Science*, 2018, **361**, 904–908.
- 99 A. Al-Ashouri, A. Magomedov, M. Roß, M. Jošt, M. Talaikis, G. Chistiakova, T. Bertram, J. A. Márquez, E. Köhnen, E. Kasparavičius, S. Levenco, L. Gil-Escrig, C. J. Hages, R. Schlatmann, B. Rech, T. Malinauskas, T. Unold, C. A. Kaufmann, L. Korte, G. Niaura, V. Getautis and S. Albrecht, Conformal monolayer contacts with lossless interfaces for perovskite single junction and monolithic tandem solar cells, *Energy Environ. Sci.*, 2019, **12**, 3356–3369.
- 100 Y. Ko, H. Park, C. Lee, Y. Kang and Y. Jun, Recent Progress in Interconnection Layer for Hybrid Photovoltaic Tandems, *Adv. Mater.*, 2020, **32**, 2002196.
- 101 L. Esaki, Long Journey into Tunneling, *Science*, 1974, **183**, 1149–1155.
- 102 M. Morales-Masis, S. D. Wolf, R. Wood-Robinson, J. W. Ager and C. Ballif, Transparent Electrodes for Efficient Optoelectronics, *Adv. Electron. Mater.*, 2017, **3**, 1600529.
- 103 D. A. Jacobs, M. Langenhorst, F. Sahli, B. S. Richards, T. P. White, C. Ballif, K. R. Catchpole and U. W. Paetzold, Light Management: A Key Concept in High-Efficiency Perovskite/Silicon Tandem Photovoltaics, *J. Phys. Chem. Lett.*, 2019, **10**, 3159–3170.
- 104 M. Jaysankar, M. Filipič, B. Zielinski, R. Schmager, W. Song, W. Qiu, U. W. Paetzold, T. Aernouts, M. Debucquoy, R. Gehlhaara and J. Poortmansabe, Perovskite–silicon tandem solar modules with optimised light harvesting, *Energy Environ. Sci.*, 2018, **11**, 1489–1498.
- 105 L. Qiu, L. K. Ono, Y. Jiang, M. R. Leyden, S. R. Raga, S. Wang and Y. B. Qi, Engineering interface structure to



- improve efficiency and stability of organometal halide perovskite solar cells, *J. Phys. Chem. B*, 2018, **122**, 511–520.
- 106 L. Qiu, Z. Liu, L. K. Ono, Y. Jiang, D.-Y. Son, Z. Hawash, S. He and Y. B. Qi, Scalable Fabrication of Stable High Efficiency Perovskite Solar Cells and Modules Utilizing Room Temperature Sputtered SnO<sub>2</sub> Electron Transport Layer, *Adv. Funct. Mater.*, 2019, **29**, 1806779.
- 107 M. R. Leyden, L. Meng, Y. Jiang, L. K. Ono, L. Qiu, E. J. Juarez-Perez, C. Qin, C. Adachi and Y. B. Qi, Methylammonium Lead Bromide Perovskite Light-Emitting Diodes by Chemical Vapor Deposition, *J. Phys. Chem. Lett.*, 2017, **8**, 3193–3198.
- 108 Y. Jiang, M. R. Leyden, L. Qiu, S. Wang, L. K. Ono, Z. Wu, E. J. Juarez-Perez and Y. B. Qi, Combination of Hybrid CVD and Cation Exchange for Upscaling Cs-Substituted Mixed Cation Perovskite Solar Cells with High Efficiency and Stability, *Adv. Funct. Mater.*, 2018, **28**, 1703835.
- 109 L. Qiu, S. He, Z. Liu, L. K. Ono, D.-Y. Son, Y. Liu, G. Tong and Y. B. Qi, Rapid hybrid chemical vapor deposition for efficient and hysteresis-free perovskite solar modules with an operation lifetime exceeding 800 hours, *J. Mater. Chem. A*, 2020, **8**, 23404–23412.
- 110 Y. Jiang, M. Remeika, Z. Hu, E. J. Juarez-Perez, L. Qiu, Z. Liu, T. Kim, L. K. Ono, D.-Y. Son, Z. Hawash, M. R. Leyden, Z. Wu, L. Meng, J.-S. Hu and Y. B. Qi, Negligible-Pb-Waste and Upscalable Perovskite Deposition Technology for High-Operational-Stability Perovskite Solar Modules, *Adv. Energy Mater.*, 2019, **9**, 1803047.
- 111 T. Moser, K. Artuk, Y. Jiang, T. Feurer, E. Gilshtein, A. N. Tiwari and F. Fu, Revealing the perovskite formation kinetics during chemical vapour deposition, *J. Mater. Chem. A*, 2020, **8**, 21973–21982.
- 112 Y. Deng, C. H. V. Brackle, X. Dai, J. Zhao, B. Chen and J. Huang, Tailoring solvent coordination for high-speed, room-temperature blading of perovskite photovoltaic films, *Sci. Adv.*, 2019, **5**, eaax7537.
- 113 M. Remeika, L. K. Ono, M. Maeda, Z. Hu and Y. B. Qi, High-throughput surface preparation for flexible slot die coated perovskite solar cells, *Org. Electron.*, 2018, **54**, 72–79.
- 114 J. B. Whitaker, D. H. Kim, B. W. Larson, F. Zhang, J. J. Berry, M. F. A. M. van Hest and K. Zhu, Scalable slot-die coating of high performance perovskite solar cells, *Sustainable Energy Fuels*, 2018, **2**, 2442–2449.
- 115 M. Remeika, S. R. Raga, S. Zhang and Y. B. Qi, Transferable optimization of spray-coated PbI<sub>2</sub> films for perovskite solar cell fabrication, *J. Mater. Chem. A*, 2017, **5**, 5709–5718.
- 116 J. E. Bishop, J. A. Smith and D. G. Lidzey, Development of Spray-Coated Perovskite Solar Cells, *ACS Appl. Mater. Interfaces*, 2020, **12**, 48237–48245.
- 117 F. Mathies, H. Eggers, B. S. Richards, G. Hernandez-Sosa, U. Lemmer and U. W. Paetzold, Inkjet-Printed Triple Cation Perovskite Solar Cells, *ACS Appl. Energy Mater.*, 2018, **1**, 1834–1839.
- 118 B. Dou, J. B. Whitaker, K. Barsten, D. T. Moore, L. M. Wheeler, J. Ryter, N. J. Breslin, J. J. Berry, S. M. Garner, F. S. Barnes, S. E. Shaheen, C. J. Tassone, K. Zhu and M. F. A. M. v. Hest, Roll-to-Roll Printing of Perovskite Solar Cells, *ACS Energy Lett.*, 2018, **10**, 2558–2565.
- 119 Y. Y. Kim, T.-Y. Yang, R. Suhonen, A. Kemppainen, K. Hwang, N. J. Jeon and J. Seo, Roll-to-roll gravure-printed flexible perovskite solar cells using eco-friendly antisolvent bathing with wide processing window, *Nat. Commun.*, 2020, **11**, 5146.
- 120 H. C. Weerasinghe, Y. Dkhissi, A. D. Scully, R. A. Caruso and Y.-B. Cheng, Encapsulation for improving the lifetime of flexible perovskite solar cells, *Nano Energy*, 2015, **18**, 118–125.
- 121 Y. Jiang, L. Qiu, E. J. Juarez-Perez, L. K. Ono, Z. Hu, Z. Liu, Z. Wu, L. Meng, Q. Wang and Y. B. Qi, Reduction of lead leakage from damaged lead halide perovskite solar modules using self-healing polymer-based encapsulation, *Nat. Energy*, 2019, **4**, 585–593.
- 122 X. Li, F. Zhang, H. He, J. J. Berry, K. Zhu and T. Xu, On-device lead sequestration for perovskite solar cells, *Nature*, 2020, **578**, 555–558.
- 123 S. Chen, Y. Deng, H. Gu, S. Xu, S. Wang, Z. Yu, V. Blum and J. Huang, Trapping lead in perovskite solar modules with abundant and low-cost cation-exchange resins, *Nat. Energy*, 2020, **5**, 1003–1011.

